Generalized Frequency Division Multiplexing for 5th Generation Cellular Networks

Nicola Michailow*, Maximilian Matthé*, Ivan Simões Gaspar*, Ainoa Navarro Caldevilla*, Luciano Leonel Mendes†*, Andreas Festag* and Gerhard Fettweis*
*Vodafone Chair Mobile Communication Systems, Technische Universität Dresden, Germany
†Instituto Nacional de Telecomunicações, Sta. Rita do Sapucai, MG, Brazil

***Abstract*—Cellular systems of the fourth generation (4G) have been optimized to provide high data rates and reliable coverage to mobile users. Cellular systems of the next generation will face more diverse application requirements: the demand for higher data rates exceeds 4G capabilities; battery-driven communication sensors need ultra-low power consumption; control applications require very short response times. We envision a unified physical layer waveform, referred to as Generalized Frequency Division Multiplexing (GFDM), to address these requirements. In this paper we analyze main characteristics of the proposed waveform and highlight relevant features. After introducing the principles of GFDM, this paper contributes to the following areas: (i) means for engineering the waveform's spectral properties, (ii) analytical analysis of symbol error performance over different channel models, (iii) concepts for MIMO-GFDM to achieve diversity, (iv) preamble-based synchronization that preserves the excellent spectral properties of the waveform, (v) bit error rate performance for channel coded GFDM transmission using iterative receivers, (vi) relevant application scenarios and suitable GFDM parameterizations, (vii) GFDM proof-of-concept and implementation aspects of the prototype using hardware platforms available today. In summary, the flexible nature of GFDM makes this waveform a suitable candidate for future 5G networks.**

***Index Terms*—5G scenarios, physical layer, non-orthogonal waveform, GFDM, pulse shaping, MIMO, synchronization, proof-of-concept.**

I. Introduction

MOBILE communication has become an essential tool for the modern society. The first generation of cellular systems provided basic, yet innovative, voice transmission. Communication started to become personal rather than being connected to fixed locations. The second generation has digitalized the voice in order to increase system capacity, battery life of devices and Quality of Service (QoS). It also introduced the Short Message Service, which revolutionized the way people communicate. The third generation enabled mobile Internet access and data rates not too far behind of wired solutions of that time. The advent of smartphones with large storage and processing capabilities equipped with high definition screen and cameras, in combination with social networks that turned users from media consumers into content providers, has pushed the fourth generation towards even higher throughput. Starting with the second generation, the evolution of the mobile communication has focused on increasing the throughput.

However, the scenarios foreseen for future fifth generation (5G) networks have requirements that clearly go beyond higher data rates [1], [2]. The main scenarios for 5G networks are *machine type communication* (MTC) [3], *Tactile Internet* [4] and *Wireless Regional Area Network* (WRAN) [5], while classical *bitpipe* communication is still considered an important application.

At present, Orthogonal Frequency Division Multiplexing (OFDM) [6] is a widely adopted solution mainly because of its robustness against multipath channels [7] and easy implementation based on Fast Fourier Transform (FFT) algorithms [8]. But the application scenarios predicted for 5G networks present challenges which OFDM can only address in a limited way. MTC and machine-to-machine (M2M) communication [9] require low power consumption, which makes the strict synchronization process required to keep the orthogonality between subcarriers unaffordable [2]. The low latency required for Tactile Internet and vehicle-to-vehicle (V2V) [10] applications demands for short bursts of data, meaning that OFDM signals with one cyclic prefix (CP) per symbol would present a prohibitive low spectral efficiency. The low spectrum efficiency due to the CP insertion is also a problem for WRAN application, where the typical channel impulse response has a duration of tenths of microseconds [11]. Additionally, the high out-of-band (OOB) emission of OFDM [12] poses a challenge for opportunistic and dynamic spectrum access [13]. All these challenges make OFDM not the most promising waveform for the next generation networks. In this context, alternative multicarrier schemes are currently being evaluated as candidates for the PHY layer of next generation of mobile communication systems.

In Filter Bank Multicarrier (FBMC) [14], one of the most investigated filtered multicarrier systems, the subcarriers are pulse shaped individually in order to reduce the OOB emissions. Because the subcarriers have narrow bandwidth, the length of the transmit filter impulse response is usually long. Typically, the filter has four times the length of the symbols. As a consequence, FBMC can only achieve good spectral efficiency if the number of transmit symbols is large. Clearly, this solution is not suitable for low latency scenarios, where high efficiency must be achieved with short burst transmissions. Universal Filtered Multicarrier (UFMC) [15] is a recent

The authors want to thank National Instruments for their generous support in making the implementation happen.

The support by Vodafone Group R&D helped create the results, and discussions shaped our ideas.

This work has been performed in the framework of the FP7 project ICT-318555 "5GNOW", which is partly funded by the European Union.

The authors would like to thank Instituto Nacional de Telecomunicações (Inatel) and Conselho Nacional de Desenvolvimento Científico e Tecnológico (CNPq Brasil) for partially funding the work presented in this paper.

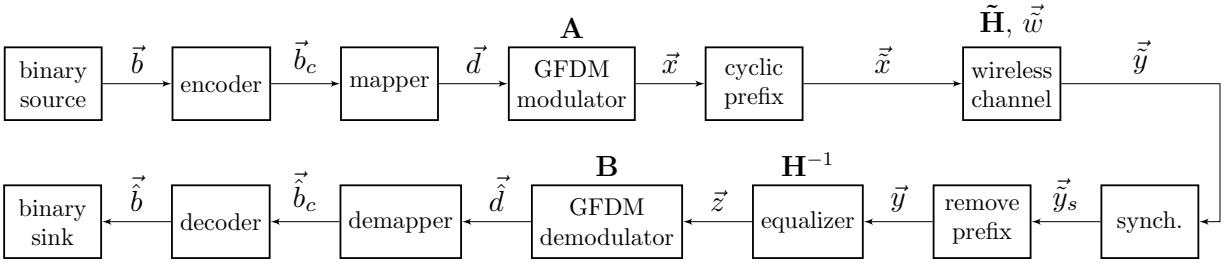

Fig. 1: Block diagram of the transceiver.

proposal where a group of subcarrier is filtered to reduce the OOB emission. Because the bandwidth of the filter covers several subcarriers, its impulse response can be short, which means that high spectral efficiency can be reached in short burst transmissions. UFMC does not require a CP and it is possible to design the filters in order to obtain a total block length equivalent to the CP-OFDM. However, because there is no CP, UFMC is more sensitive to small time misalignment than CP-OFDM [15]. Hence, UFMC might not be suitable for applications that require loose time synchronization in order to save energy. Bi-orthogonal Frequency Division Multiplexing (BFDM) [16] employs well localized pulse shapes at the transmitter and receiver side that are bi-orthogonal to each other. The good frequency-localization of the transmit pulse makes the system robust against frequency dispersion (Doppler effect) while the good time-localization of the pulse provides robustness against time dispersion (multipath). Nevertheless, the Balian-Low theorem prohibits time-frequency well-localized pulses when using standard Quadrature Amplitude Modulation (QAM) with maximum spectral efficiency [17]. Therefore, BFDM employs Offset QAM (OQAM) to achieve well localized pulses both in time and frequency domains. Hence, critically dense BFDM cannot be easily integrated with MIMO aiming diversity [18], which is one of the key points for 5G applications. Also, similar to FBMC, BFDM needs to handle long pulse tails that reduces the efficiency for short burst transmission necessary in low latency and M2M applications.

A flexible multicarrier modulation scheme, named Generalized Frequency Division Multiplexing (GFDM) [19], has also been proposed for the air interface of 5G networks. The flexibility of GFDM allows it to cover CP-OFDM and single-carrier frequency domain equalization (SC-FDE) [20] as special cases. GFDM is based on the modulation of independent blocks, where each block consist of a number of subcarriers and subsymbols. The subcarriers are filtered with a prototype filter that is circularly shifted in time and frequency domain. This process reduces the OOB emissions, making fragmented spectrum and dynamic spectrum allocation feasible without severe interference in incumbent services or other users. The subcarrier filtering can result in non-orthogonal subcarriers and both inter-symbol interference (ISI) and inter-carrier interference (ICI) might arise. Nevertheless, efficient receiving techniques can eliminate this interference, i.e. a matched filter receiver with iterative interference cancellation [21] can achieve the same symbol error rate (SER) performance as OFDM over different channel models.

GFDM is a promising solution for the 5G PHY layer because its flexibility can address the different requirements. For real-time applications, the signal length must be reduced to fulfill certain latency requirements [10]. Because GFDM is confined in a block structure of MK samples, where K subcarriers carry M subsymbols each, it is possible to design the time-frequency structure to match the time constraints of low latency applications. Different filter impulse responses can be used to filter the subcarriers and this choice affects the OOB emissions and the SER performance. As will be shown, GFDM allows engineering signals in their frequency and time characteristics. Thus, the scheme retains all main benefits of OFDM at the cost of some additional implementation complexity.

In a GFDM block, the overhead is kept small by adding a single CP for an entire block that contains multiple subsymbols. This benefit can be used to improve the spectral efficiency of the system or it can be traded for an additional cyclic suffix (CS), which allows to relax the synchronization requirements of multiple users in an MTC scenario [2]. Furthermore, all major synchronization algorithms developed for OFDM [22] can be adapted for GFDM. Of course, multiple input multiple output (MIMO) [23] will be a key feature in 5G networks. In this paper we show that space-time coding (STC) [24] can be effectively combined with GFDM for achieving transmit and receive diversity.

Though the increased complexity of GFDM will surely be manageable with the evolution of electronics, our proposed scheme can be implemented with today's technology already. A flexible, customizable Field Programmable Gate Array (FPGA) platform [25] has been used to develop a GFDM proof-of-concept and testbed for experimental research. An efficient receiver structure is employed to implement the matched filter or zero-forcing receivers based on any prototype filter.

This work contributes with the following new aspects: We present a detailed description and numerical evaluation of two techniques that improve the spectral properties of GFDM, namely inserting guard symbols and pinching the block boundaries. SER performance is investigated with new analytical expressions for the AWGN, frequency-selective and time-variant channel. A way of applying space time coding to GFDM is proposed, which allows for full diversity gain despite the fact that the waveform is non-orthogonal. Techniques to synchronize the receiver which are known from OFDM are

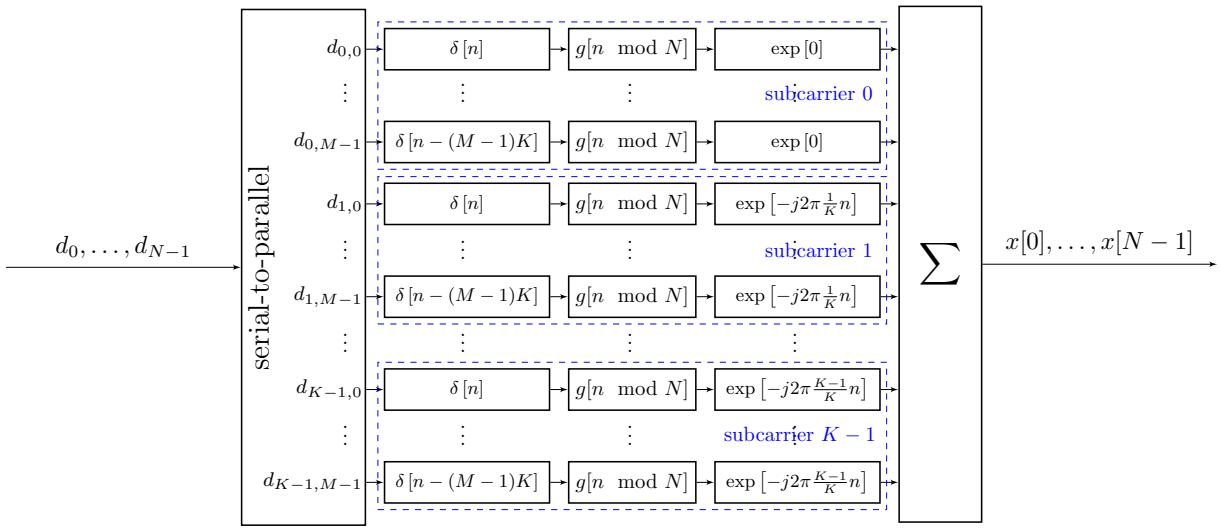

Fig. 2: Details of the GFDM modulator.

adapted to GFDM. But, in this case, additionally the constraint of preserving the good spectral properties of the waveform is addressed. The bit error rate performance of linear and iterative GFDM receivers is evaluated in combination with error control coding. Several sets of GFDM parameters are presented, which serve as a guideline how to configure the transmitter and receiver such that it can address the four 5G application scenarios. And lastly, an efficient receiver architecture is presented that enables to implement receive filters with arbitrary bandwidth.

The remaining sections are organized as follows: Section II presents basic principles of GFDM, highlighting the modulation and demodulation procedures. Section III presents the waveform engineering for GFDM, where several prototype filters are analyzed in terms of OOB emissions. Section IV analyzes the SER performance of GFDM, including theoretic equations, assuming zero-forcing receiver under different channel models. OOB emission vs. noise enhancement is also analyzed in this section. Section V combines time-reversal STC with GFDM to achieve diversity over time-variant frequency-selective channels. Section VI provides solutions for time and frequency domain synchronization, based on state-of-art approaches developed for OFDM. Section VII extends the basic matched filter receiver by successive interference cancellation (SIC) and compares its performance in a coded system. In Section VIII, it is shown how GFDM can be parameterized in order to meet the channel and application requirements for different scenarios. Section IX describes a case of study of a proof-of-concept receiver setup. Finally, Section X concludes the paper.

II. System Description and Properties

Consider the block diagram depicted in Fig. 1. A data source provides the binary data vector $\vec{b}$, which is encoded to obtain $\vec{b}_c$. A mapper, e.g. QAM, maps the encoded bits to symbols from a 2^μ-valued complex constellation where μ is the modulation order. The resulting vector $\vec{d}$ denotes a data block that contains N elements, which can be decomposed into K subcarriers with M subsymbols each according to $\vec{d} = \left(\vec{d_0}^{\mathrm{T}}, \ldots, \vec{d_{M-1}}^{\mathrm{T}}\right)^{\mathrm{T}}$ and $\vec{d}_m = (d_{0,m}, \ldots, d_{K-1,m})^{\mathrm{T}}$. The total number of symbols follows as $N = KM$. Therein, the individual elements $d_{k,m}$ correspond to the data transmitted on the kth subcarrier and in the mth subsymbol of the block. The details of the GFDM modulator are shown in Fig. 2. Each $d_{k,m}$ is transmitted with the corresponding pulse shape

$$g_{k,m}[n] = g\left[(n - mK) \mod N\right] \cdot \exp\left[-j2\pi\frac{k}{K}n\right], \quad (1)$$

with n denoting the sampling index. Each $g_{k,m}[n]$ is a time and frequency shifted version of a prototype filter $g[n]$, where the modulo operation makes $g_{k,m}[n]$ a circularly shifted version of $g_{k,0}[n]$ and the complex exponential performs the shifting operation in frequency. The transmit samples $\vec{x} = (x[n])^{\mathrm{T}}$ are obtained by superposition of all transmit symbols

$$x[n] = \sum_{k=0}^{K-1}\sum_{m=0}^{M-1} g_{k,m}[n]d_{k,m}, \quad n = 0, \ldots, N-1. \quad (2)$$

Collecting the filter samples in a vector $\vec{g}_{k,m} = (g_{k,m}[n])^{\mathrm{T}}$ allows to formulate (2) as

$$\vec{x} = \mathbf{A}\vec{d}, \quad (3)$$

where $\mathbf{A}$ is a $KM \times KM$ transmitter matrix [26] with a structure according to

$$\mathbf{A} = \begin{pmatrix}\vec{g}_{0,0} & \ldots & \vec{g}_{K-1,0} & \vec{g}_{0,1} & \ldots & \vec{g}_{K-1,M-1}\end{pmatrix}. \quad (4)$$

Fig. 3 shows three columns of an example transmitter matrix. As one can see, $\vec{g}_{1,0} = [\mathbf{A}]_{n,2}$ and $\vec{g}_{0,1} = [\mathbf{A}]_{n,K+1}$ are circularly frequency and time shifted versions of $\vec{g}_{0,0} = [\mathbf{A}]_{n,1}$.

At this point, $\vec{x}$ cointains the transmit samples that correspond to the GFDM data block $\vec{d}$. Lastly, on the transmitter side a cyclic prefix of N_{CP} samples is added to produce $\vec{\tilde{x}}$.

Transmission through a wireless channel is modelled by $\vec{\tilde{y}} = \tilde{\mathbf{H}}\vec{\tilde{x}} + \vec{\tilde{w}}$, where $\vec{\tilde{y}}$ is the received counterpart of $\vec{\tilde{x}}$. Here, $\tilde{\mathbf{H}}$ denotes the channel matrix which is

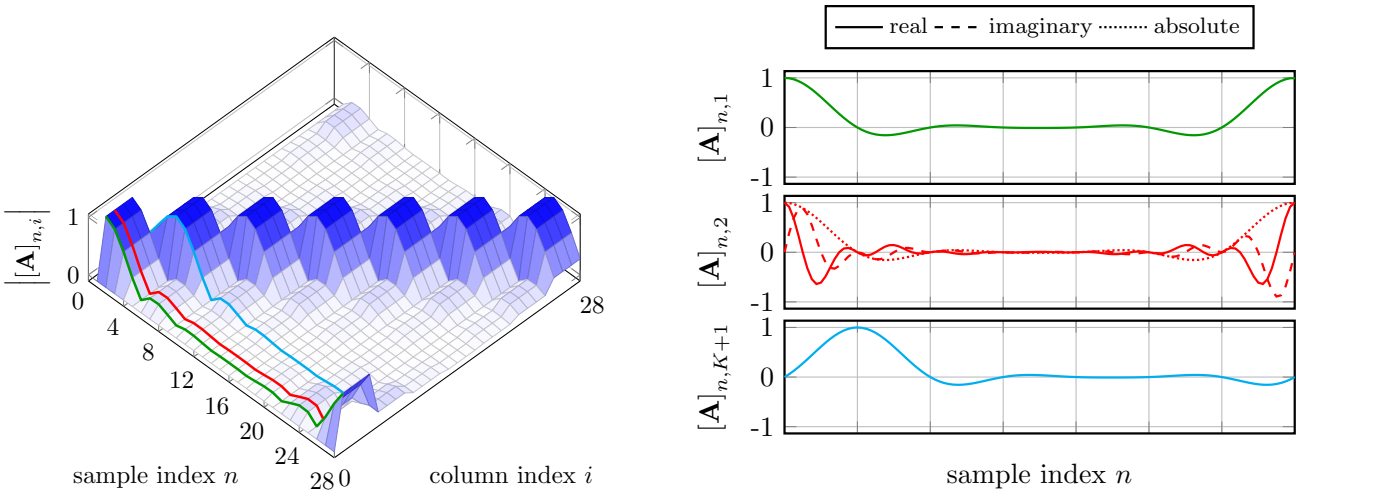

(a) A transmitter matrix.

(b) Three columns in detail.

Fig. 3: Illustration of GFDM transmitter matrix for $N = 28$, $K = 4$, $M = 7$ and a raised cosine (RC) filter with roll-off 0.4.

a $N + N_{\text{CP}} + N_{\text{ch}} - 1$ by $N + N_{\text{CP}}$ convolution matrix with band-diagonal structure based on a channel impulse response $\vec{h} = (h_0, \ldots, h_{N_{\text{ch}}-1})^{\text{T}}$ of length N_{ch}. Lastly, $\vec{w} \sim \mathcal{CN}\left(\mathbf{0}, \sigma_w^2 \mathbf{I}_{N+N_{\text{CP}}+N_{\text{ch}}-1}\right)$ denotes additive white Gaussian noise (AWGN). At the receiver, time and frequency synchronization is performed, yielding $\vec{y}_{\text{s}}$. Then the cyclic prefix is removed. Under the assumption of perfect synchronization, i.e. $\vec{y}_{\text{s}} = \vec{y}$, the cyclic prefix can be utilized to simplify the model of the wireless channel to

$$\vec{y} = \mathbf{H}\vec{x} + \vec{w}, \tag{5}$$

by replacing $\tilde{\mathbf{H}}$ with the N by N matrix $\mathbf{H}$, which is the corresponding circular convolution matrix. This allows employing zero-forcing channel equalization as efficiently used in OFDM [6], although other equalization procedures can be employed [27]. The overall transceiver equation can be written as $\vec{y} = \mathbf{H}\mathbf{A}\vec{d} + \vec{w}$. Introducing $\vec{z} = \mathbf{H}^{-1}\mathbf{H}\mathbf{A}\vec{d} + \mathbf{H}^{-1}\vec{w} = \mathbf{A}\vec{d} + \vec{\tilde{w}}$ as the received signal after channel equalization, linear demodulation of the signal can be expressed as

$$\hat{\vec{d}} = \mathbf{B}\vec{z}, \tag{6}$$

where $\mathbf{B}$ is a $KM \times KM$ receiver matrix. Several standard receiver options for the GFDM demodulator are readily available in literature: The *matched filter* (MF) receiver $\mathbf{B}_{\text{MF}} = \mathbf{A}^{\text{H}}$ maximizes the signal-to-noise ratio (SNR) per subcarrier, but with the effect of introducing self-interference when a non-orthogonal transmit pulse is applied, i.e. the scalar product $\langle g_{0,0}, g_{k,m} \rangle_{\mathbb{C}^N} \neq \delta_{0,k}\delta_{0,m}$ with Kronecker delta $\delta_{i,j}$. The *zero-forcing* (ZF) receiver $\mathbf{B}_{\text{ZF}} = \mathbf{A}^{-1}$ on the contrary completely removes any self-interference at the cost of enhancing the noise. Also, there are cases in which $\mathbf{A}$ is ill-conditioned and thus the inverse does not exist. The linear *minimum mean square error* (MMSE) receiver $\mathbf{B}_{\text{MMSE}} = (\mathbf{R}_w^2 + \mathbf{A}^{\text{H}}\mathbf{H}^{\text{H}}\mathbf{H}\mathbf{A})^{-1}\mathbf{A}^{\text{H}}\mathbf{H}^{\text{H}}$ makes a trade-off between self-interference and noise enhancement. Here, $\mathbf{R}_w^2$ denotes the covariance matrix of the noise. Note that in case of MMSE reception, the channel is jointly equalized in the receiving process, hence the zero-forcing channel equalizer block is not required and $\hat{\vec{d}} = \mathbf{B}\vec{y}$. Finally, the received symbols $\hat{\vec{d}}$ are demapped to produce a sequence of bits $\hat{\vec{b}}_{\text{c}}$ at the receiver, which are then passed to a decoder to obtain $\hat{\vec{b}}$.

From the description of the transmitter and receiver, it can be concluded that GFDM falls into the category of filtered multicarrier systems. The name derives from the fact that the scheme offers more degrees of freedom than traditional OFDM or single carrier with SC-FDE. GFDM turns into OFDM when $M = 1$, $\mathbf{A} = \mathbf{F}_N^{\text{H}}$ and $\mathbf{B} = \mathbf{F}_N$, where $\mathbf{F}_N$ is a $N \times N$ Fourier matrix. SC-FDE is obtained when $K = 1$ and SC-FDM, a frequency division multiplexing of several SC-FDE signals, is obtained when $\vec{g}$ is a Dirichlet pulse [28]. However, the important property that distinguishes the proposed scheme from OFDM and SC-FDE is that, like SC-FDM, it allows dividing a given time-frequency resource into K subcarriers and M subsymbols as depicted in Fig. 4. Therefore, it is possible to engineer the spectrum according to given requirements and enables pulse shaping on a per subcarrier basis. As a consequence, without changing the sampling rate, GFDM can be configured to cover a portion of bandwidth either with a large number of narrow band subcarriers like in OFDM or with a small number of subcarriers of large individual bandwidth like in SC-FDM. Further it is important to note that although filters are introduced, GFDM is still a block based approach. These aspects are relevant for the scheduling of users in a multiple access scenario [2] and also when targeting low latency transmissions [4].

III. Waveform Engineering

The flexibility of GFDM allows designing a signal that has a very low OOB radiation. This section contains a theoretic analysis of the OOB radiation of GFDM. The main contribution is a detailed description and numeric evaluation of techniques for reducing OOB radiation..

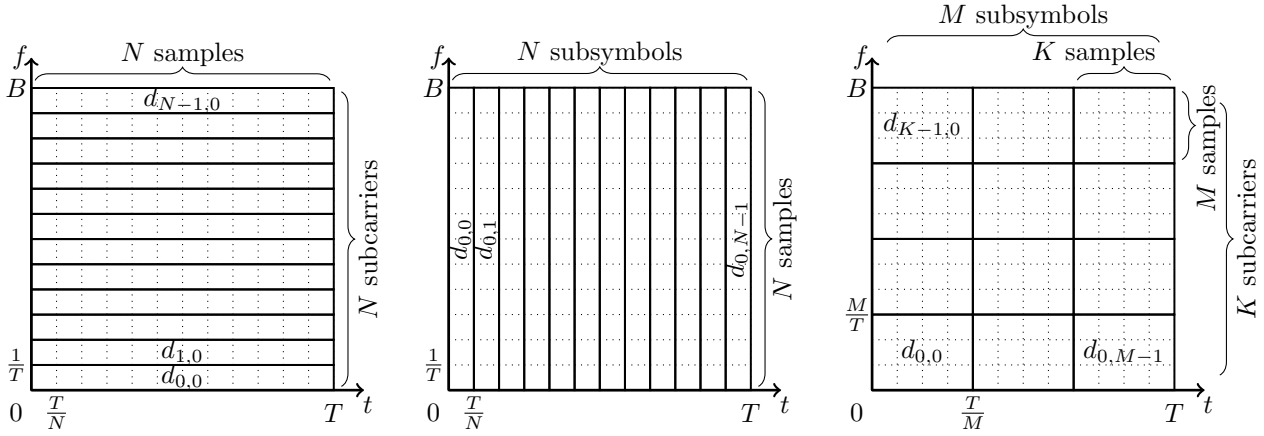

(a) OFDM (b) SC-FDE (c) SC-FDM and GFDM

Fig. 4: Partitioning of time and frequency, where data occupies different resources depending on the chosen scheme. (a) with $K = N$ subcarriers and $M = 1$ subsymbols, (b) with $K = 1$ subcarriers and $M = N$ subsymbols and (c) with $K = 4$, $M = 3$ and $N = 12$.

The choice of the pulse shaping filters strongly influences the spectral properties of the GFDM signal and the symbol error rate. The frequency responses of candidate filters employed are summarized in Tab. I(a), whereas the respective impulse responses are calculated by inverse discrete Fourier transform (IDFT). In Tab I(a), $\mathrm{lin}_\alpha(x)$ is a truncated linear function with $\mathrm{lin}_\alpha(x) = \min\left(1, \max\left(0, \frac{1+\alpha}{2\alpha} + \frac{|x|}{\alpha}\right)\right)$ that is used to systematically describe the roll-off area defined by α in the frequency domain. Further, $p_4(x) = x^4(35 - 84x + 70x^2 - 20x^3)$ is a polynomial that maps the range $(0, 1)$ onto itself.
In GFDM, the kth subcarrier is centered at the normalized frequency k/K and hence, α describes the overlap of the subcarriers in the frequency domain. In particular, for $\alpha = 0$ all functions in Tab. I(a) reduce to a rect and are denoted the Dirichlet filter [29, p. 619], since the impulse response is the Mth Dirichlet kernel of the discrete Fourier transform (DFT) of length MK. Fig. 5 shows sample impulse and frequency responses of the described pulse shaping filters.

To measure the OOB radiation, the power spectral density (PSD) of the baseband signal can be formulated as [30]

$$P(f) = \lim_{T\to\infty}\left(\frac{1}{T}E\{|\mathcal{F}\{x_T(t)\}|^2\}\right), \tag{7}$$

where $x_T(t)$ is the transmit signal that is truncated to the interval $(-T/2, T/2)$. In GFDM, $x_T(t)$ is the concatenation of multiple GFDM blocks

$$x_T(t) = \sum_{v,m,k} d_{vmk} g_{0m}(t - vMT_s) e^{-j2\pi\frac{k}{T_s}t} \tag{8}$$

with respective Fourier transform given by

$$X_T(f) = \sum_{v,m,k} d_{vmk} G_m\left(f - \frac{k}{T_s}\right) e^{-j2\pi vMT_s f} \tag{9}$$

where T_s is the time duration of one subsymbol, v is the block index that ranges from $-\frac{T}{2MT_s}$ to $+\frac{T}{2MT_s}$, and k, m range over all allocated subcarriers and subsymbols. When assuming i.i.d. data symbols with unit variance, inserting (9) into (7) yields the PSD of the GFDM system as

$$P(f) = \frac{1}{MT_s}\sum_{k,m}\left|G_m\left(f - \frac{k}{T_s}\right)\right|^2. \tag{10}$$

The OOB radiation of the GFDM signal is defined as the ratio between the amount of energy that is emitted into the frequency range $\mathcal{OOB}$ and the amount of energy within the allocated bandwidth $\mathcal{B}$ by

$$O = \frac{|\mathcal{B}|}{|\mathcal{OOB}|}\cdot\frac{\int_{f\in\mathcal{OOB}} P(f)df}{\int_{f\in\mathcal{B}} P(f)df}. \tag{11}$$

Between $\mathcal{B}$ and $\mathcal{OOB}$ a number of guard subcarriers is inserted. Fig. 6(a) illustrates the concept of guard subcarriers for OOB measurement and shows a comparison of the PSD of OFDM and GFDM. By default, due to the abrupt changes of the signal value between GFDM blocks, the OOB radiation of GFDM is approximately $15\,\mathrm{dB}$ below OFDM. In order to make the pulse shaping even more effictive in reducing the OOB radiation, two suitable techniques are discussed:
1) *Inserting Guard Symbols (GS)*: When using an ISI-free transmission filter (e.g. the RC or Xia filters) and CP with length of $rK, r \in \mathbb{N}$ samples, it is possible to keep the signal value constant at the block boundaries by setting the 0th and $(M - r)$th subsymbol to a fixed value. Fig. 6(a) shows the strongly attenuated OOB radiation of GFDM, when the GS value is set to zero, denoted by GS-GFDM. For high M the reduction of the spectral efficiency by $\frac{M-2}{M}$ due to the GS insertion can be neglected and furthermore, these subsymbols are free for inserting synchronization signals and pilots. In case of high M, increase of latency can be mitigated by proportionally reducing the subsymbol duration and enlarging the subcarrier bandwidth. The number of subcarriers can be reduced, in order to keep the occupied bandwidth constant.
2) *Pinching the Block Boundary*: The insertion of the CP of N_{CP} samples introduces redundancy in the transmitted data. In windowed GFDM (W-GFDM) this is exploited at the transmitter side by multiplying each GFDM block with a

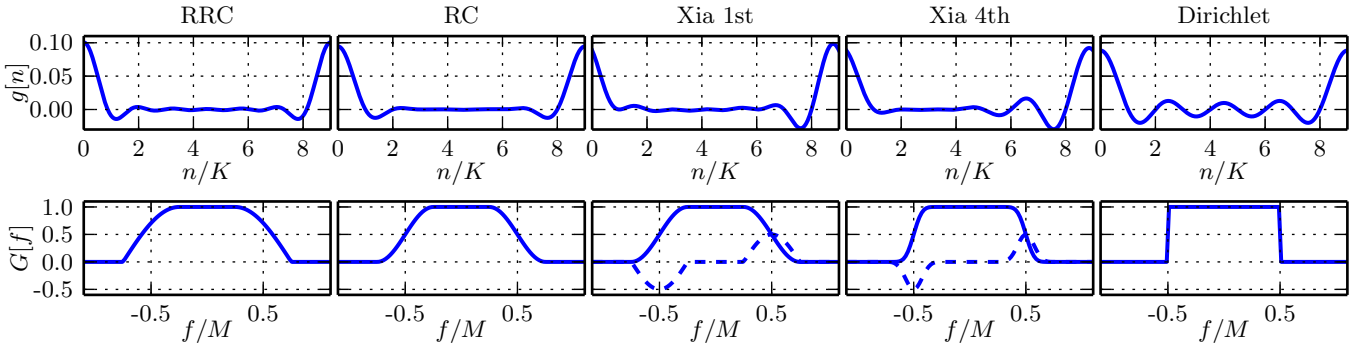

Fig. 5: Impulse and frequency response of employed pulse shaping filters. Roll-off α is set to 0.5 except for the Dirichlet filter ($\alpha = 0$). Solid and dashed lines denote real and imaginary part, respectively.

TABLE I: Pulse shaping filters and window functions.

(a) Investigated pulse shaping filters.

Name	Frequency response
RC	$G_{\text{RC}}[f] = \frac{1}{2}\left[1 - \cos(\pi \,\text{lin}_\alpha(\frac{f}{M}))\right]$
Root RC	$G_{\text{RRC}}[f] = \sqrt{G_{RC}[f]}$
1st Xia [31]	$G_{\text{Xia}}[f] = \frac{1}{2}\left[1 - e^{-j\pi \,\text{lin}_\alpha(\frac{f}{M})\,\text{sign}(f)}\right]$
4th Xia [31]	$G_{\text{Xia4}}[f] = \frac{1}{2}\left[1 - e^{-j\pi p_4(\text{lin}_\alpha(\frac{f}{M}))\,\text{sign}(f)}\right]$

(b) Window functions for block pinching.

Window	Time domain
Rect	$w_{\text{Rect}}[n] = 1$
Ramp	$w_{\text{R}}[n] = \text{lin}_{\frac{N_{\text{W}}}{KM}}\left[\frac{KM+N_{\text{W}}}{2KM}\left(\frac{2n}{KM+N_{CP}} - 1\right)\right]$
RC	$w_{\text{RC}}[n] = \frac{1}{2}\left[1 - \cos(\pi w_R[n])\right]$
4th RC	$w_{\text{RC4}}[n] = \frac{1}{2}\left[1 - \cos(\pi p_4(w_R[n]))\right]$

window function $w[n]$ in the time domain to provide a smooth fade-in and fade-out as illustrated in Fig. 6(c). Different window functions are given in Tab. I(b), where N_{W} is the number of samples that are included in the linear part of the ramp $w_R[n]$. At the receiver side, the data is recovered from the received W-GFDM block by summing the parts of the CP that were modified by the window. As a result, a noise enhancement of $10\log_{10}(1 + \frac{N_{\text{W}}}{KM})$ dB occurs because of the summation of two redundant parts of the signal. This noise enhancement can be mitigated by using the square root of the block window at the transmitter and at the receiver which resembles the matched filter approach. Calculations of the OOB power have been carried out with the parameters in Tab. II, where different CP lengths have been employed. The results for one and six guard carriers are shown in Fig. 6(b). Obviously, any of the presented GFDM configurations has a lower OOB radiation than OFDM. GS-GFDM efficiently reduces the OOB radiation to 32 dB below OFDM with a CP of K samples. For a CP length of $K/4$, GS-GFDM performs 20 dB below OFDM. Pinching is most effective in combination with a higher number of guard carriers, since the multiplication with a block window spreads the spectrum of the GFDM signal. The w_{RC4}-window attenuates the OOB radiation with six guard carriers most, but has the least suppression with one guard carrier due to its wide mainlobe in the frequency domain. It can attenuate the OOB radiation to below -100 dB as is shown in Fig. 6(b) in the solid blue line. When tolerating six guard carriers, the pinching technique can supress the OOB radiation below -70 dB with a ramp length of only a quarter subsymbol and an RC window.

IV. Symbol Error Rate Performance Analysis

In this section we analyze the performance of the GFDM system in terms of SER versus E_s/N_0 assuming that a ZF receiver is employed. This type of linear receiver is able to remove self-generated interference at the cost of introducing noise enhancement, depending on the pulse shape. Differently from previous work, where the bit error rates have been analyzed only based on simulations [26], this section introduces analytical expression to evaluate the GFDM SER performance under AWGN, static frequency-selective channels (FSC) and flat time-variant channels (TVC). Besides the SER performance analysis, this section provides a trade-off analysis between noise enhancement and OOB emissions for different pulse shapes.

The system parameters used for the simulation are presented in Tab. II, while Tab. III shows the channel impulse response used in the SER performance evaluation. Fig. 7(a) shows

TABLE II: Simulation parameters.

Parameter	**Value**
Mapping	16-QAM
Transmit Filter	RC
Roll-off (α)	0.1 or 0.9
Number of subcarriers (K)	64
Number of subsymbols (M)	9
CP length (N_{CP})	16 samples
CS length (N_{CS})	0 samples

the receive filter impulse response for ZF and MF receivers assuming the parameters presented in Tab. II with $\alpha = 0.9$ to highlight the noise enhancement. Fig. 7(b) shows the cor-

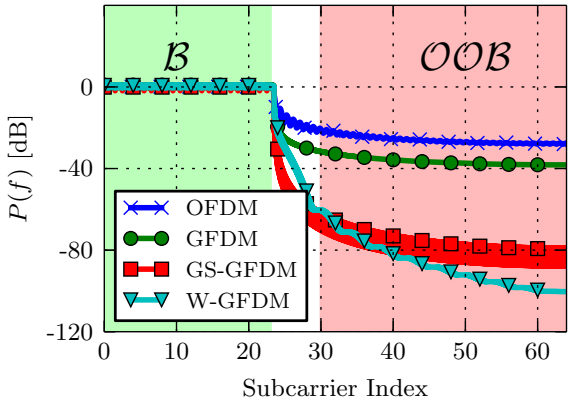

(a) PSD of OFDM and GFDM. GFDM employs a CP of length of one subsymbol and the pinching is done with a RC window with $W = K/4$. Regions that are considered in-band and out-of-band are marked with $\mathcal{B}$ and $\mathcal{OOB}$, respectively and in between both ranges a number of guard carriers is considered.

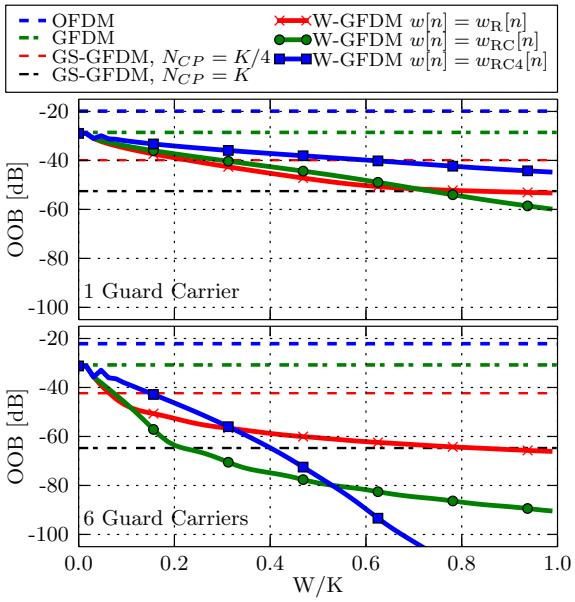

(b) OOB radiation of different GFDM configurations

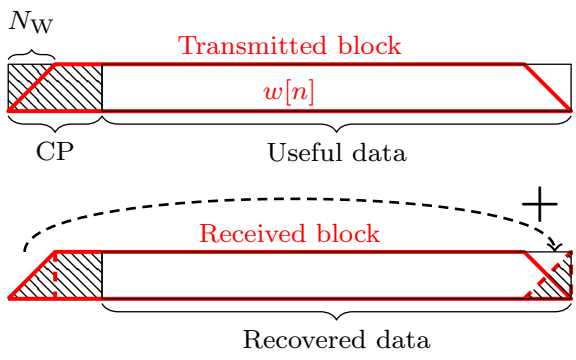

(c) Pinching the block boundary yields W-GFDM.

Fig. 6: Waveform engineering results.

TABLE III: Channel impulse response and delay spread for the considered channel models.

Channel	Impulse Response	Delay Spread
AWGN	$\vec{h} = (1)$	$N_{\mathrm{ch}} = 1$
FSC	$\vec{h} = \left(10^{\frac{-i}{N_{\mathrm{ch}}-1}}\right)^{\mathrm{T}}_{i=0,\ldots,N_{\mathrm{ch}}-1}$	$N_{\mathrm{ch}} = N_{\mathrm{CP}}$
TVC	$\vec{h} = (h)$, $h \sim \mathcal{CN}(0,1)$	$N_{\mathrm{ch}} = 1$

responding frequency response of both filters. As visible, the ZF filter collects noise outside the desired bandwidth, affecting the SER performance of the system. Over flat channels, the noise enhancement factor (NEF) ξ determines the signal-to-noise ratio (SNR) reduction when using the ZF receiver. It is defined as

$$\xi = \sum_{n=0}^{MK-1} \left| [\mathbf{B}_{\mathrm{ZF}}]_{k,n} \right|^2, \tag{12}$$

which is equal for every k.

1) *AWGN Channel*: The NEF adjusts the equivalent SNR for GFDM at the receiver side. Consequently, GFDM and OFDM SER performance under AWGN [32] only differs in the equivalent SNR. Therefore, GFDM SER under AWGN is given by

$$\begin{aligned} p_{\mathrm{AWGN}}(e) = 2\left(\frac{\kappa-1}{\kappa}\right)\mathrm{erfc}\left(\sqrt{\gamma}\right) + \\ - \left(\frac{\kappa-1}{\kappa}\right)\mathrm{erfc}^2\left(\sqrt{\gamma}\right), \end{aligned} \tag{13}$$

where

$$\gamma = \frac{3R_T}{2(2^{\mu}-1)} \cdot \frac{E_s}{\xi N_0}, \tag{14}$$

and

$$R_T = \frac{KM}{KM + N_{\mathrm{CP}} + N_{\mathrm{CS}}}, \tag{15}$$

μ is the number of bits per QAM symbol, $\kappa = \sqrt{2^{\mu}}$, N_{CP} and N_{CS} are the length of cyclic prefix and cyclic suffix (CS) respectively, E_s is the average energy per symbol, and N_0 is the noise power density.

Fig. 8(a) compares the SER performance of GFDM and OFDM under AWGN taking the energy spent for CP into account. The figure shows that the pulse shape and, consequently the NEF, plays an important role in the GFDM performance. The noise enhancement can be neglected when a RC filter with $\alpha = 0.1$ is used and, in this case, the GFDM and OFDM SER curves match. For this reason, only the theoretical OFDM curve has been plotted in Fig. 8.a. On the other hand, the GFDM SER performance is severely degraded due to noise enhancement when a RC filter with $\alpha = 0.9$ is used. The prototype pulse shape must be properly chosen in order to avoid prohibitive performance loss due to noise enhancement. Fig. 8(a) also shows that GFDM suffers a smaller performance penalty due to the CP insertion when compared with OFDM. The GFDM performance gain over OFDM is given by

$$\eta = 10\log\left[\frac{M(K + N_{\mathrm{CP}} + N_{\mathrm{CS}})}{MK + N_{\mathrm{CP}} + N_{\mathrm{CS}}}\right] \quad \mathrm{dB}. \tag{16}$$

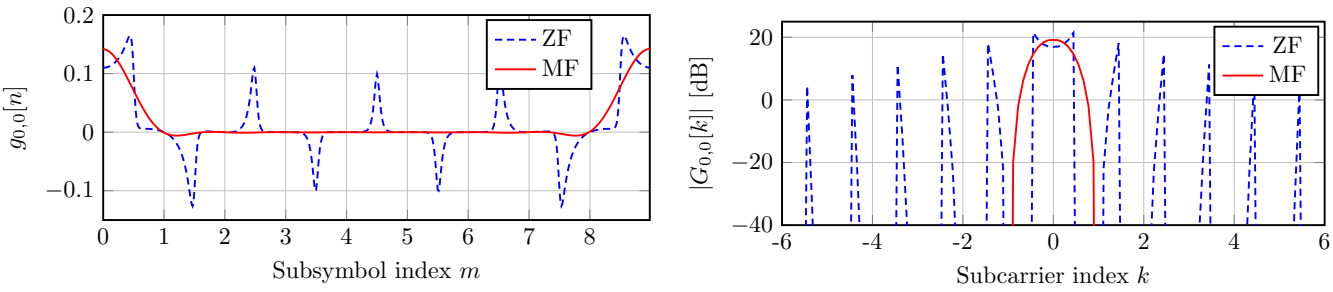

(a) Impulse response

(b) Frequency response

Fig. 7: Time and frequency characteristics of the ZF and MF receiving filters.

Hence, a large M must be chosen if spectrum efficiency is an important requirement in the system design. On the other hand, it must be noted that latency increases linearly with M in this case. Therefore, when choosing the length of the CP, a trade-off between latency and spectrum efficiency must be found for given applications.

2) *Frequency-selective channel*: A good SER performance over FSCs is an important requirement for multicarrier modulations. Following the block diagram presented in Fig. 1, the signal at the input of the demapper when the ZF receiver is employed is given by

$$\vec{\tilde{d}} = \vec{d} + \vec{w}_{eq}, \tag{17}$$

where

$$\vec{w}_{eq} = \mathbf{BF}^{-1}\frac{\vec{W}}{\vec{H}} \tag{18}$$

is the equivalent noise, $\vec{W}$ is the noise vector in the frequency domain, and $\vec{H}$ is the vector of the channel frequency response. The variance of the equivalent noise for the lth subcarrier can be evaluated from (18) and leads to

$$\sigma_l^2 = \frac{1}{MK}\sum_{k=0}^{MK-1}\left|\frac{G_{R_{l,m}}[-k]}{H[k]}\right|^2 \sigma_n^2 = \xi_l\sigma_n^2 = \xi_l\frac{N_0}{2}, \tag{19}$$

where $G_{R_{l,m}}[k]$ is the frequency response of the filter for the lth subcarrier and mth subsymbol and ξ_l is the corresponding NEF. Notice that σ_l^2 is equal for every m. The position of the filter in the frequency domain changes the NEF because the channel frequency response is not flat for multipath channels. Hence, the GFDM SER over FSCs is given by

$$\begin{aligned} p_{\text{FSC}}(e) = 2\left(\frac{\kappa-1}{\kappa K}\right)\sum_{l=0}^{K-1}\text{erfc}\left(\sqrt{\gamma_l}\right) + \\ -\frac{1}{K}\left(\frac{\kappa-1}{\kappa}\right)^2\sum_{l=0}^{K-1}\text{erfc}^2\left(\sqrt{\gamma_l}\right), \end{aligned} \tag{20}$$

where

$$\gamma_l = \frac{3R_T}{2(2^\mu-1)}\cdot\frac{E_s}{\xi_l N_0}. \tag{21}$$

GFDM has M times more samples per subcarrier when compared to OFDM, which provides a higher spectrum resolution for equalization, allowing GFDM to better mitigate the frequency selectivity per subcarrier.

Fig. 8(b) compares the performance of GFDM and OFDM over FSC considering the channel delay profile presented in Tab. III with $N_{\text{ch}} = 16$. Again, GFDM uses the CP more efficiently when compared to OFDM. Notice that the channel delay profile leads to a coherence bandwidth of $\mathcal{B}_{\text{c}} \approx f_s/259$ and the bandwidth of each subcarrier is $\mathcal{B}_{\text{sc}} \approx f_s/64$, which means that this channel is frequency-selective per subcarrier. In this scenario, the larger number of samples per subcarriers allows GFDM to present a better performance than OFDM, as shown in Fig. 8(b). In fact, for high SNR, the GFDM performance when employing an RC filter with $\alpha = 0.9$ and large NEF approaches the OFDM SER.

3) *Time-variant channel*: In a time-variant channel both instantaneous SNR and instantaneous SER are random variables. Thus, the average symbol error probability over a time-variant channels is an important tool to analyse the system performance. Consider that a time-variant channel can be modelled as a multiplicative channel where the amplitude gain is a Rayleigh random variable with parameter σ_r and phase uniformly distributed between $-\pi$ and π. It is assumed that the channel remains static during the transmission of one GFDM symbol. In this case, the GFDM SER follows the OFDM SER with the penalty of the noise enhancement when a ZF receiver is employed. Due to the flat property of the channel, the NEF is constant for all subcarriers. Therefore, the SER of GFDM over time-variant channels is given by

$$\begin{aligned} p_{\text{TVC}}(e) = 2\left(\frac{\kappa-1}{\kappa}\right)\left(1-\sqrt{\frac{\gamma_r}{1+\gamma_r}}\right) + \\ -\left(\frac{\kappa-1}{\kappa}\right)^2\left[1-\frac{4}{\pi}\sqrt{\frac{\gamma_r}{1+\gamma_r}}\text{atan}\left(\sqrt{\frac{1+\gamma_r}{\gamma_r}}\right)\right], \end{aligned} \tag{22}$$

where

$$\gamma_r = \frac{3\sigma_r^2 R_T}{2^\mu-1}\frac{E_s}{\xi N_0}. \tag{23}$$

Fig. 8(c) shows the GFDM and OFDM SER performance assuming a Rayleigh channel with parameter $\sigma_r^2 = \frac{1}{2}$. Once again, we can observe that the NEF resulting from the chosen pulse shape is neglectable when compared with OFDM for $\alpha = 0.1$. GFDM benefits from using only one CP for M subsymbols, which results in a better power and spectral efficiency.

Closed-form solutions for the SER performance under AWGN of the matched filter receiver are available in [33]. The MF receiver outperforms the ZF receiver in low SNR regions due to the significant influence of the noise enhancement.

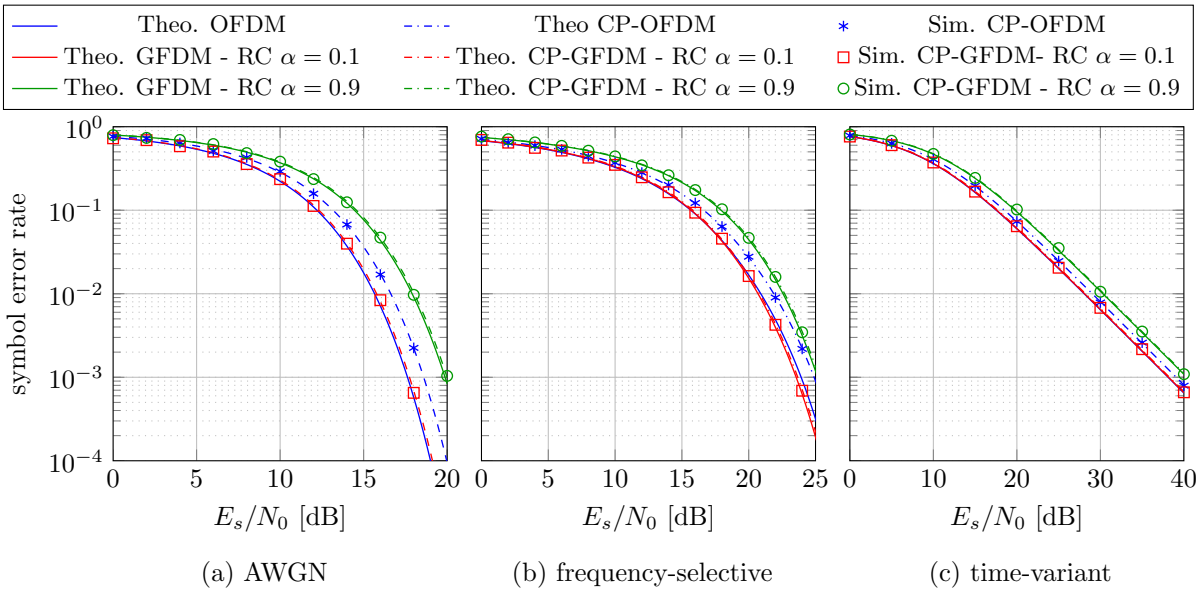

Fig. 8: GFDM and OFDM SER performance in different channels. The minimum number of symbol errors for each SNR value is: 500 for AWGN and frequency-selective channels and 20000 for time-variant channel.

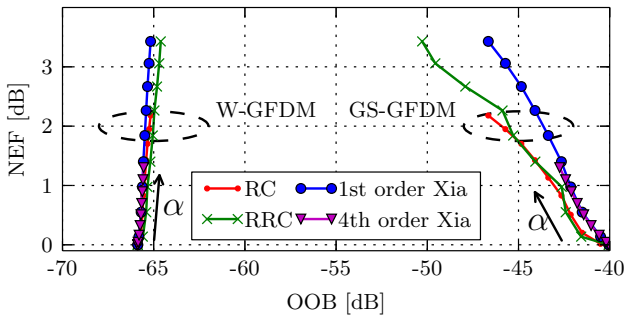

Fig. 9: NEF and OOB for various GFDM filters. OOB radiation was measured with 6 guard carriers. The W-GFDM system uses a RC window with a ramp length of $K/4$. The roll-off α increases in the direction of the arrows from 0 to 1 in steps of 0.1.

However, since the MF receiver suffers from self-interference, it cannot reach the performance of the ZF approach at high SNR values. The MMSE receiver balances the noise enhancement and self-interference so that it converges to the MF receiver for low SNR and to the ZF receiver for high SNR regions. However, no closed form solutions for the SER in Rayleigh fading channels do exist. Simulated SER curves for the MMSE receiver are provided in [26]. Fig. 9 shows the OOB radiation and NEF of different filters and different roll-off factors for W-GFDM and GS-GFDM assuming the system parameters presented in Table II. The choice of the pulse shaping filter significantly influences the NEF and, in case of GS-GFDM, also the OOB radiation. For W-GFDM the OOB radiation is nearly independent of the employed filter. The NEF increases with the roll-off factor due to the wider overlapping of the subcarriers. The ZF receiver needs to put more effort into ICI cancellation which is bought for an increased NEF in the range from $0\,\mathrm{dB}$ for the Dirichlet filter up to $3.5\,\mathrm{dB}$ for full roll-off RRC and 1st order Xia filters. The 4th order Xia filter shows the lowest NEF of $1.25\,\mathrm{dB}$ with full roll-off. However, for practical applications, the RC and 4th order Xia filter with lower α in the range of $0 \leq \alpha \leq 0.2$ are preferrable.

V. Space-Time Coded GFDM

Any 5G system shall be able to exploit the benefits of multiple transmit and receive antennas. Transmission diversity [24] is a crucial feature for future wireless networks to achieve the required reliability and robustness under frequency-selective and time-variant channels. Due to the orthogonality of the symbols the Alamouti-STC is easily applied in OFDM [34]. For GFDM, the overlapping subsymbols in the time domain impede the direct application of the Alamouti-STC within one GFDM block. However, as a major contribution of this section, we show that the block-structure of GFDM enables the application of time-reversal STC, which has been developed for single carrier systems to achieve diversity under frequency-selective channels [35]. Fig. 10 presents the block diagrams of the STC-GFDM transmitter and receiver.

In this approach, two data vectors $\vec{d}_1$ and $\vec{d}_2$ are independently modulated leading to

$$\vec{x}_1 = \mathbf{A}\vec{d}_1 \quad \text{and} \quad \vec{x}_2 = \mathbf{A}\vec{d}_2. \tag{24}$$

The modulated signals are delivered to the space-time encoder to produce the signals that will be transmitted by the two antennas in two successive time frames, which are presented in Tab. IV. A CP is appended to each signal before transmission.

TABLE IV: STC signals.

	Antenna 1	**Antenna 2**
Time frame 1	$x_{11}[n] = x_1[n]$	$x_{21}[n] = -x_2^*[-n \mod N]$
Time frame 2	$x_{12}[n] = x_2[n]$	$x_{22}[n] = x_1^*[-n \mod N]$

On the receiver side, the signals at the ith receiving antenna

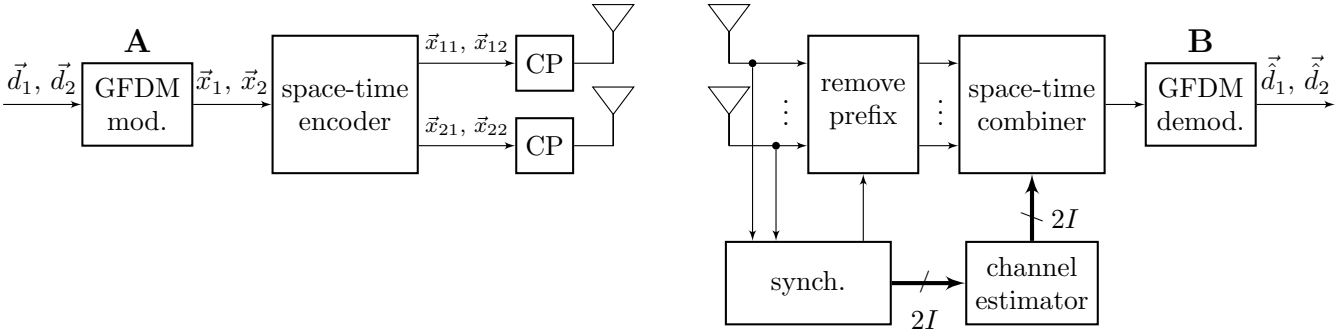

Fig. 10: Transceiver block diagram of the STC-GFDM.

on time frames 1 and 2 are given by

$$\begin{aligned}\vec{y}_{i1} &= \mathbf{H}_{1i}\vec{x}_{11} + \mathbf{H}_{2i}\vec{x}_{21} + \vec{w}_{i1} \\ \vec{y}_{i2} &= \mathbf{H}_{1i}\vec{x}_{12} + \mathbf{H}_{2i}\vec{x}_{22} + \vec{w}_{i2},\end{aligned} \tag{25}$$

where $\mathbf{H}_{ji}$ is the circulant matrix with the impulse response of the channel between the jth transmitting antenna and the ith receiving antenna, and $\vec{w}_{i1}$ and $\vec{w}_{i2}$ are the noise vectors received by ith receiving antenna in the time frames 1 and 2, respectively. It is assumed that the channel coherence time is larger than two GFDM symbols.

The space-time maximum ratio combining is carried out in the frequency domain to achieve diversity. The combined signals in the frequency domain are given by

$$\begin{aligned}\hat{\vec{X}}_1 &= \frac{\sum_{i=1}^{I} \mathbf{\Xi}_{1i}^* \vec{Y}_{i1} + \mathbf{\Xi}_{2i} \vec{Y}_{i2}^*}{\sum_{i=1}^{I} \mathbf{\Xi}_{1i}^* \mathbf{\Xi}_{1i} + \mathbf{\Xi}_{2i}^* \mathbf{\Xi}_{2i}} \\ &= \vec{X}_1 + \frac{\sum_{i=1}^{I} \mathbf{\Xi}_{1i}^* \vec{W}_{i1} + \mathbf{\Xi}_{2i} \vec{W}_{i2}^*}{\sum_{i=1}^{I} \mathbf{\Xi}_{1i}^* \mathbf{\Xi}_{1i} + \mathbf{\Xi}_{2i}^* \mathbf{\Xi}_{2i}} = \vec{X}_1 + \vec{W}_{eq_1} \\ \hat{\vec{X}}_2 &= \frac{\sum_{i=1}^{I} \mathbf{\Xi}_{1i}^* \vec{Y}_{i2} - \mathbf{\Xi}_{2i} \vec{Y}_{i1}^*}{\sum_{i=1}^{I} \mathbf{\Xi}_{1i}^* \mathbf{\Xi}_{1i} + \mathbf{\Xi}_{2i}^* \mathbf{\Xi}_{2i}} \\ &= \vec{X}_2 + \frac{\sum_{i=1}^{I} \mathbf{\Xi}_{1i}^* \vec{W}_{i2} - \mathbf{\Xi}_{2i} \vec{W}_{i1}^*}{\sum_{i=1}^{I} \mathbf{\Xi}_{1i}^* \mathbf{\Xi}_{1i} + \mathbf{\Xi}_{2i}^* \mathbf{\Xi}_{2i}} = \vec{X}_2 + \vec{W}_{eq_2}\end{aligned} \tag{26}$$

where I is the number of receiving antennas, $\mathbf{\Xi}_{ji} = \mathbf{F}\mathbf{H}_{ji}\mathbf{F}^{-1}$ and $\vec{Y}_{i1}$ and $\vec{Y}_{i2}$ are the discrete Fourier transform of $\vec{y}_{i1}$ and $\vec{y}_{i2}$, respectively.

The estimated data vectors can be obtained from the combined signals presented in (26), therefore

$$\hat{\vec{d}}_j = \mathbf{B}\mathbf{F}^{-1}\hat{\vec{X}}_j. \tag{27}$$

Fig. 11 compares the SER performance of classical STC-OFDM [34] with STC-GFDM considering the system parameters from Tab. II and the frequency selective channel delay profile from Tab. III, however, each tap of the channel impulse response is multiplied by i.i.d. Rayleigh random variables with parameter $\sigma_r^2 = \frac{1}{2}$. Also, the total transmitting power is kept constant, which means that each antenna transmits with half of the available power. Two transmitting antennas and two receiving antennas have been used in this simulation. Fig. 11 shows that STC-GFDM and STC-OFDM achieve the same diversity gain. In a practical system setup, α shall be chosen small because the NEF can be neglected. Again, STC-GFDM uses the CP more efficiently which leads to a better

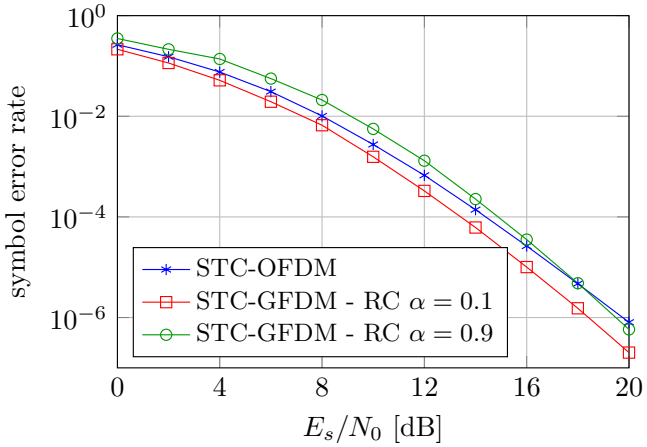

Fig. 11: SER performance of the 2x2 STC-OFDM and STC-GFDM under frequency-selective and time-variant channel. The minimal number of symbol errors for each SNR value is 20000.

performance than STC-OFDM when small α is used. The NEF becomes significant for high values of α, resulting in a performance loss. Nevertheless, the diversity gain of $2I$ is achieved by STC-GFDM for both transmit pulses analyzed in this section. As stated in Sec. IV, GFDM has a higher spectrum resolution per subcarrier, which allows for a better frequency domain equalization. The benefit of a more precise equalization can be also observed in Fig. 11, where the slopes of the STC-GFDM curves are steeper than for STC-OFDM. Hence, even STC-GFDM employing RC with $\alpha = 0.9$ performs better than STC-OFDM for high SNR ($E_s/N_0 > 18$ dB).

VI. Block Based Synchronization

Synchronization is a key element in the performance of the signal processing carried out on receivers and can be achieved in GFDM on a block basis. The block structure with its CP allows adaptation of fundamental OFDM solutions to estimate symbol time offset (STO) and carrier frequency offset (CFO) [36], [37], but low OOB is a factor to be specifically considered in GFDM.

The algorithm proposed in [22] will be evaluated in this section to achieve one-shot synchronization using a straightforward proposal of a separated W-GFDM preamble, which is defined with $M = 2$ and the transmitted data in the kth subcarriers

of both subsymbols $d_{k,0}$ and $d_{k,1}$ are filled with the same pseudo-noise (PN) sequence, resulting in a signal composed with two identical halves.
Low OOB is obtained by pinching the block boundary and Fig. 12 illustrates this configuration, where a W-GFDM preamble precedes another W-GFDM data block and forms a burst with a double pinching pattern. As described in Sec. III, different pinching lengths N_{Wp} and N_{Wd} can be applied respectively to the preamble and data blocks in order to achieve a desired emission mask.

Given that $r[n]$ is a set of received samples containing at least one complete W-GFDM preamble, the two identical halves are identified with an autocorrelation metric, which is integrated along the CP and CS length to remove plateau effects [37], [38], leading to the metric

$$\mu[n] = \sum_{\iota=-N_{\mathrm{CP}}}^{0} \sum_{k=0}^{N-1} r[n+\iota+k]^* r\left[n+\iota+k+\frac{N}{2}\right]. \quad (28)$$

The argument that maximizes the absolute value of the metric $\mu[n]$ is taken as a coarse STO

$$\hat{n}_{\mathrm{c}} = \underset{n}{\operatorname{argmax}} |\mu[n]|, \quad (29)$$

while the angle of $\mu[\hat{n}_{\mathrm{c}}]$ is used to estimate the CFO as

$$\hat{\epsilon} = \frac{\angle \mu[\hat{n}_{\mathrm{c}}]}{\pi}. \quad (30)$$

The value $\hat{\epsilon}$ is employed to correct the CFO in the received sequence and a cross-correlation operation is then performed as

$$c[n] = \frac{1}{N} \sum_{k=0}^{N-1} r[n+k]^* e^{j2\pi \frac{\hat{\epsilon}}{N}(n+k)} p[k], \quad (31)$$

where $p[k]$ represents the known GFDM preamble.
To suppress side peaks that arise from the two halves and from the CP and CS parts, $c[n]$ is combined with $\mu[n]$ and an optimized estimation of the STO is obtained by searching the peak value in the range around the coarse STO estimation $[\hat{n}_{\mathrm{c}} - \frac{N}{2},\ \hat{n}_{\mathrm{c}} + \frac{N}{2}]$ that is

$$\hat{n}_{\mathrm{o}} = \underset{n}{\operatorname{argmax}} \ \left(|c[n]||\mu[n]|\right). \quad (32)$$

This synchronization procedure is robust for single path channels, but in a time-variant FSC, the primary echo can be lower than other echoes and the strongest peak will not represent the correct STO. Thus, an additional search before $\hat{n}_{\mathrm{o}}$ can reveal if there is another yet undetected peak to be considered as the primary one. For samples that do not belong to the preamble, the output of the cross-correlation can be interpreted as a complex Gaussian random sequence and a threshold criteria, depending on an acceptable probability of false alarm p_{FA}, can reveal the presence of multipaths before $\hat{n}_{\mathrm{o}}$.
Considering that the first peak of (31) is within the range $(\hat{n}_{\mathrm{o}} - \lambda,\ \hat{n}_{\mathrm{o}}]$, where $\lambda < N_{\mathrm{CP}}$ is an adjustable parameter, the threshold is defined as

$$T_{\mathrm{Th}} = \sqrt{-\frac{4}{\pi}\ln\left(p_{\mathrm{FA}}\right)} \left(\frac{1}{\frac{N}{2} - 2\lambda} \sum_{k=-\frac{N}{2}+\lambda}^{-\lambda} |c[\hat{n}_{\mathrm{o}} + k]| \right) \quad (33)$$

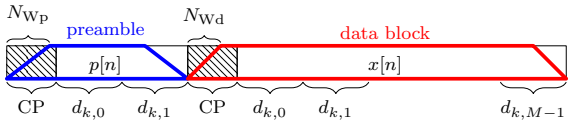

Fig. 12: W-GFDM preamble preceding a W-GFDM data block.

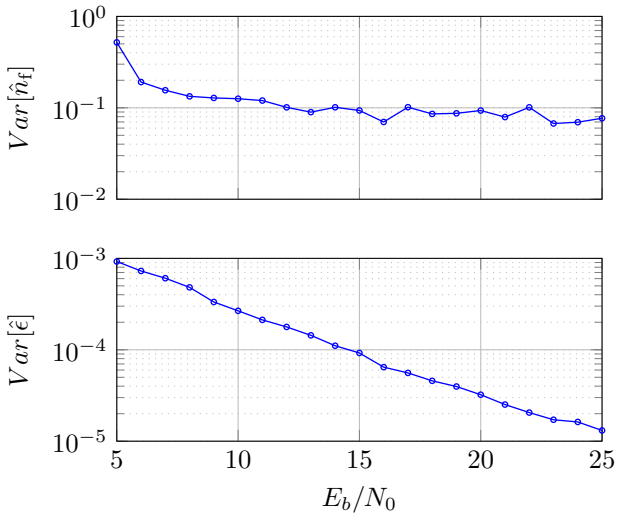

Fig. 13: Performance evaluation of variance of the fine STO estimation $\hat{n}_{\mathrm{f}}$ and CFO estimation $\hat{\epsilon}$ for the GFDM preamble in a time-variant multipath channel

and the fine STO estimation for the first multipath is finally given by

$$\hat{n}_f = \underset{\hat{n}_{\mathrm{o}}-\lambda<n\leq\hat{n}_{\mathrm{o}}}{\operatorname{argfirst}} \ \left(|c[n]| > T_{\mathrm{Th}}\right). \quad (34)$$

The performance evaluation in terms of variance of normalized STO and CFO estimations is presented in Fig. 13 for the W-GFDM preamble following the parameters presented in Table II but with $M = 2$. A $w_{RC}[n]$ window function with $N_{\mathrm{W}} = 16$ is used, $\lambda = 16$, $p_{\mathrm{FA}} = 10^{-4}$ and the time-variant FSC is set as described in Sec. V. For a SNR range higher than 5 dB the variance of the STO estimation stabilizes within tenths of a sample due the time variant fading effect in the multipath channel. The variance of the CFO estimation starts from thousandths of the subcarrier bandwidth and gets linearly better (in log scale) with increasing SNR.
The results obtained with the double pinching configuration show that burst synchronization can be achieved without penalties to the performance when compared with the results presented in [22]. The smooth block boundaries at the edges of the preamble and the data portion of the signal are particularly important as keeping OOB emission low is an important feature of GFDM.

VII. Advanced Receiver

In this section, the previously presented basic matched filter approach is extended by successive interference cancellation (SIC) [21], yielding the MF-SIC receiver. We investigate its performance compared to the ZF and to the linear MMSE receiver in terms of bit error rates (BER). Compared to the previous work, error control coding is introduced in the the

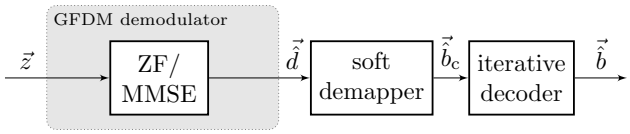

(a) ZF and MMSE receiver configuration

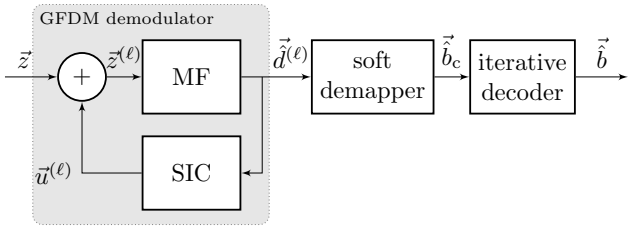

(b) MF-SIC receiver configuration

Fig. 14: The considered receiver configurations.

setup. The results show that although ZF can severely enhance the noise in the system, it can be a reasonable alternative to the iterative approach in some cases, mainly when small values of α and M are employed.

A non-orthogonal waveform like GFDM inherently introduces correlation across all subcarriers and subsymbols within a block, which can result in unwanted self-interference among the elements of $\vec{\hat{d}}$, when the MF receiver is employed. Supposed ℓ is the iteration index, the algorithm starts by first detecting all data symbols $\vec{\hat{d}}^{(\ell)}$, $\ell = 0$ based on the received signal $\vec{z}$. In the first iteration $\ell = 1$, the detected data symbols $\vec{\hat{d}}^{(0)}$ are then fed back to calculate a cancellation signal $\vec{u}_{k,m}^{(\ell)} = \mathbf{A}\vec{\hat{d}}^{(\ell-1)} - \vec{g}_{k,m}\hat{d}_{k,m}$ for each pair of (k,m), which is based on all but the (k,m)th element of $\vec{\hat{d}}^{(\ell-1)}$. The received and equalized signal $\vec{z}$ is partially cleaned of interference, producing $\vec{z}_{k,m}^{(\ell)} = \vec{z} + \vec{u}_{k,m}^{(\ell)}$. Lastly, the (k,m)th data symbol is detected again to obtain $\hat{d}_{k,m}^{(\ell)}$. The ℓth iteration is complete once all pairs of (k,m) are run through. The total number of SIC iterations shall be denoted by J_{SIC}.

This method has been shown to be effective, even for high order of QAM mapping [39]. However, for large K and M this can significantly increase the computational complexity of the receiver. In this case, using a Nyquist filter allows to elimininate self-intersymbol-interference and thus requires to iterate only through the subcarriers in the system. Another option is to define a threshold for $\langle \vec{g}_{k',m'}, \vec{g}_{k,m} \rangle$ with $k \neq k'$ and $m \neq m'$, below which $d_{k',m'}$ is considered not to have influence on $\hat{d}_{k,m}$.

Additionally, an interesting question is, to what degree can coding help to overcome the impairments of the non-orthogonal waveform. To investigate this, encoder and decoder are introduced in the transmission chain. The parallel concatenated convolutional code (PC-CC) from [40] with code rate $R = 1/3$ is considered for this section. On the receiver side, a turbo decoder [41] with J_{TD} iterations is employed.

In the following, the two configurations depicted in Fig. 14 shall be considered. In the first setup, a linear receiver, i.e. ZF or linear MMSE, is utilized in combination with the turbo decoder. The second setup employs MF with several SIC iterations prior to decoding. As a reference, an orthogonal SC-FDM transmission is used. The performance is compared in terms of bit error rates in AWGN, frequency-selective and time-variant channels from Tab. III and the configuration of the GFDM system is based on Tab. II.

The main objective here is to evaluate the penalty of using a non-orthogonal waveform. Generally, when the transmit filter exhibits little self-interference ($\alpha = 0.1$), for either of MF and ZF, the PC-CC alone is able to close the gap to the orthogonal system. In a situation where the interference becomes severe ($\alpha = 0.9$), MF and ZF can strongly deviate from the performance of the orthogonal system. Looking at the AWGN case, noise enhancement appears to have a more severe impact than the self-interference as MF outperforms ZF. However, with increasing E_b/N_0 in the frequency selective channel, the MF can only outperform the ZF, when combined with SIC. This behaviour is similar in the time-variant channel, however here a pronounced waterfall region is absent. In the case of strong self-interference, the performance of the MMSE receiver is comparable to MF-SIC for the time-variant channel, while MF-SIC outperforms it by $0.5\,\text{dB}$ for high SNR in AWGN conditions and by an even smaller fraction of that in the frequency-selective channel.

Overall, it can be concluded that when operating with little self-interference, ZF should be favored as ZF and MF-SIC show nearly identical performance, but ZF does not entail the complexity overhead of the SIC iterations. When self-interference is severe, MF-SIC outperforms at the cost of more computational effort. The MMSE achieves similar performance as the ZF receiver, when looking at the frequency-selective or the time-variant channel.

VIII. Application Requirements

New scenarios are being foreseen for 5G networks with requirements that cannot be addressed only with throughput increment. In this section, we present a short description of the most prominent application scenarios and propose sets of GFDM parameters to address the specific requirements. In particular, adequate values of K and M based on the restrictions from the wireless channel characteristics and on the requirements of the application scenarios are established. Table V presents the typical channel parameters and a suggested GFDM configuration for each scenario. The application scenarios considered in this section are:

1) *Bitpipe communication*: Currently broadcasting services are experiencing a media shift, where television and radio content are being broadcasted through the Internet. People demand their favorite shows anywhere, and smartphones and tablets are commonly used to access the content. With screen resolution on mobile devices beyond high definition, videos and 3D contents will require several tens of Mbps to achieve a good Quality of Experience (QoE). Therefore, next generation networks must rely on advanced digital communication techniques, such as MIMO [23] for diversity and multiplexing, highly efficient channel coding, small cell coverage with inter-cell interference management and efficient dynamic spectrum allocation. For

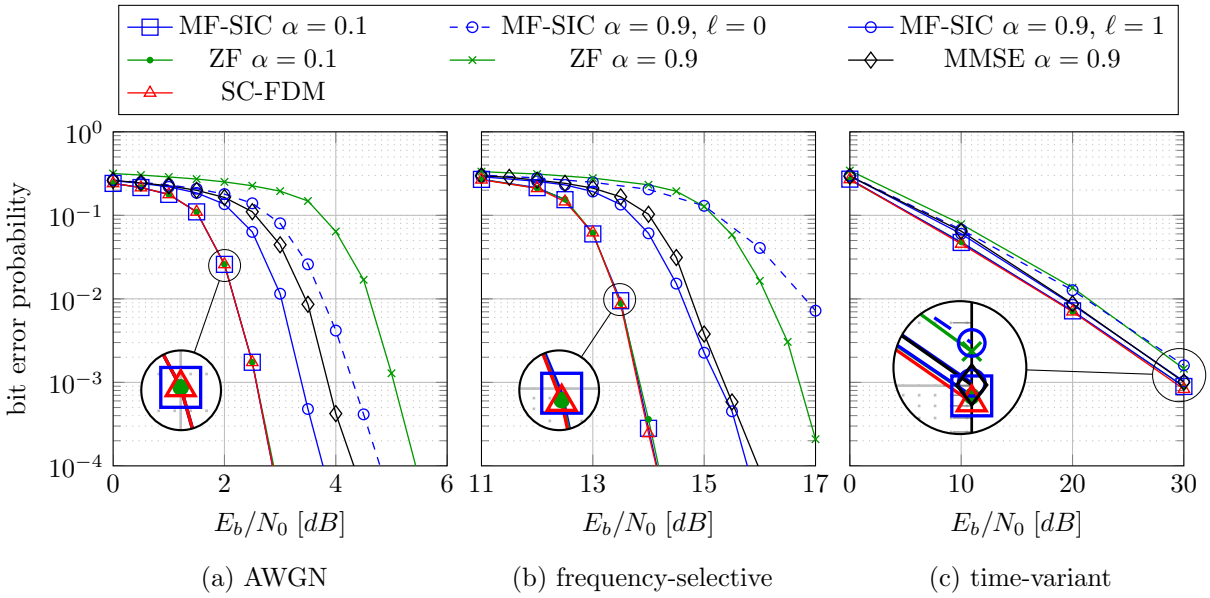

(a) AWGN (b) frequency-selective (c) time-variant

Fig. 15: BER simulation results for a coded system with $J_{\text{TD}} = 10$ and $J_{\text{SIC}} = 1$.

waveform engineering, low out-of-band emission is a crucial requirement to allow fragmented and opportunistic spectrum allocation with cognitive radios (CR) [42]. Orthogonal Frequency Division Multiplexing (OFDM) [6] with $-35\,\text{dBc}$ OOB emissions will hardly be able to attend the emission mask without additional filtering, which renders the deployment of OFDM questionable in the next generation standards.

As presented in Section IV, GFDM can achieve OOB emission several dBs below OFDM and, therefore, is more suitable to explore vacant and fragmented spectrum. Besides the low OOB emission, GFDM configuration with large M can reduce the impact of the CP length in the overall throughput and can significantly increase the spectrum efficiency. GFDM combined with Coordinated Multipoint transmission [43] can increase the spectrum re-use in small cell networks without increasing the interference between cells.

2) *Machine Type Communication (MTC)*: Machines, devices and even objects are becoming intelligent and equipped with sensors, which increasingly allow them to operate autonomously and to communicate without human interaction. While today's MTC is mainly based on short-range wireless technologies, such as Bluetooth and Zigbee, it is expected that cellular systems providing wide area coverage will gain a significant market share. There are two major markets foreseen for MTC. The first considers machines as complete systems with only an interface that allows for controlling it over the Internet. The other considers machines as sensors and actuators where all the control system is to be moved to a cloud infrastructure. Although the first approach can be implemented shortly, the second one is regarded as the most interesting because the connected sensors will provide accurate information for Big Data processing [44], allowing for data analytics to uncover patterns and correlations, and offer new or better services. Consider a scenario, where smart devices in a given environment communicate among each other or with a central station without human intervention. These devices

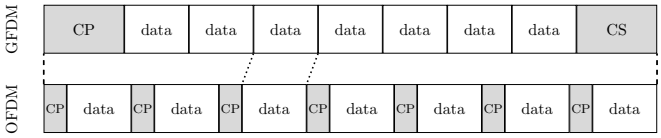

Fig. 16: GFDM and OFDM frame comparison for the MTC scenario.

are typically powered by batteries and their lifetime must be extended. MTC devices connecting to cellular networks cannot pass through all the synchronization steps, because this process would consume a large amount of energy. Hence, MTC devices must be able to achieve reliable communication with a loose synchronization or even operate asynchronously. A large CP and CS can be used to allow for loose time domain synchronization in a random access channel [15], but this approach cannot be efficiently used with OFDM as it requires one CP and CS per symbol. GFDM applies one CP and one CS in a block with several subsymbols. Therefore, a LTE resource block can be organized as a GFDM block with CP and CS large enough to accommodate timing misalignment (see Figure 16). It is worth noting that GFDM is able to increase the size of the CP and introduce a CS without consuming further resources when compared with the LTE approach.

3) *Tactile Internet*: This new application scenario is first envisioned in [4], where the 5G network is used for real-time control applications with at most $1\,\text{ms}$ round-trip latency requirements. The low latency requirement is determined by the typical interaction latency for tactile steering and control of real and virtual objects. In fact, most of today's mobile devices use a touch screen as input interface and future devices will integrate various interfaces for haptic, visual and auditory input and feedback. These new interface devices are also going to be used to interact with the online environment for virtual and augmented reality, health monitoring, smart house controlling, gaming and many different applications. If too

TABLE V: Channel and system parameters for the identified application scenarios.

Parameters	**Bitpipe**	**Tactile Internet**	**MTC**	**WRAN**
Cell size [km]	4	1	4	100
Delay Spread [μs]	5	1	5	50
$\mathcal{B}_\mathrm{c}$ [kHz]	40	200	40	4
Doppler shift [Hz]	100	10	100	10
T_c [ms]	5	50	5	50
Subcarriers K	$2^{0,1,2,\ldots,8}$	64 or 128	1	$2^{0,1,\ldots,4}$
Subsymbols M	1023 ... 5	5	7	1023 ... 127
Receiver type	MF-SIC	ZF	ZF	MF-SIC
T_CP [μ]	7	2	7	80
Symbol duration [μs]	≤ 5000	≈ 5	≈ 500	≤ 50000
Modulation order	2, 4, 6 or 8	2 or 4	2	2, 4, 6 or 8
$\mathcal{B}_\mathrm{w}$ [MHz]	20	100 (Fragmented)	1	5, 10 or 20

large, the round-trip delays between the command insertion, the action in the online environment and the feedback can result in a poor QoE or even cybersickness. Since the overall round-trip system delay cannot be larger than $1\,\mathrm{ms}$, the time budget for the physical layer will be of no more than hundreds of μs. The current frame structure of Long Term Evolution (LTE), based on $70\,\mu\mathrm{s}$ OFDM symbols, has a latency that is at least one order of magnitude above the target for the Tactile Internet. GFDM can address this application by having a small MK product. This approach will lead to larger bandwidth per subcarrier, which means that each one might suffer from channel frequency-selectiveness. Nevertheless, because GFDM has M samples per subcarrier, FDE can be applied in this case.

4) *WRAN*: Despite the fact that reasonable Internet access is available in cities, sparsely populated areas suffer from low data rate and unreliable solutions. Wired technologies have limited coverage and require large investments. Today's wireless networks have relatively small cell size and operate in licensed frequencies, which makes them economical unfeasible in low populated areas. CR technology addresses this problem by dynamically and opportunistically accessing vacant UHF TV bands. When using OFDM as the air interface, it is a challenge to attend the emission mask imposed by spectrum regulation. Besides this, large cell coverage leads to high delay spread and the conventional OFDM with a CP for every symbol will result in a low spectral efficiency. The next generation network shall address large coverage areas using dynamic channel allocation based on CR with low OOB emissions and efficiently deal with the multipath effects by reducing the impact of the CP in the overall data rate.

Although a long CP is requested to avoid ISI, in this scenario the user terminals are typically static and Doppler effect plays a small role. Slow time-variant channels allow for GFDM blocks with large M, whereas the increased latency is not critical to the WRAN application scenarios and CP and CS can be efficiently used to avoid ISI and time misalignment.

In general, the channel characteristics, such as coherence time (T_c) and coherence bandwidth ($\mathcal{B}_\mathrm{c}$), impose a restriction to the number of subsymbols and subcarriers. The coherence time defines an upper boundary for MK, while the coherence bandwidth defines a lower bound according to

$$\frac{R_\mathrm{s}}{\mathcal{B}_c}(1+\alpha) < MK < T_\mathrm{c} R_\mathrm{s}, \tag{35}$$

where R_s is the overall symbol rate.

In summary, flexibility will be one key aspect for future cellular systems in order to address the wide range of foreseen application scenarios. GFDM in particular can address the requirements of these application scenarios where the configuration of the number of subcarriers and subsymbols is an important feature.

IX. Prototype Implementation

The GFDM scheme has been implemented as proof-of-concept on a FPGA based platform. The theoretical foundations for the transceiver algorithms are provided in [39] and [45]. Both, the transmitter and the receiver implementation exploit the fact that the corresponding filters are limited to L subcarriers in the frequency domain and this section explores a way of realizing values $L > 2$ on the receiver side. In order to utilize the parallel processing capabilities of the FPGA in a pipelining structure, the transmit and receiver filter frequency responses are split into L groups of M samples according to

$$\begin{aligned} F[k] &= \mathrm{DFT}_{LM}\left\{(-1)^n g\left[\tfrac{K}{L} n\right]\right\} \\ F_l[j] &= F[lM + j], \end{aligned} \tag{36}$$

where $k = 0, \ldots, LM-1$, $j = 0, \ldots, M-1$, $g[n]$ is the impulse response of the prototype transmit or receive filter, the factor $\frac{K}{L}$ corresponds to a decimation in time, and $(-1)^n$ causes a FFT shift in the frequency domain. At the transmitter the standard RC and Xia filters limited to $L = 2$ are implemented. The frequency response of the receiver filter depends on the receiver type. For a small α it can be reasonably limited to $L = 2$ and $L = 16$ for the MF and ZF receiver, respectively (cf. Fig. 7). The main contribution of this section is to present a receiver structure that is not limited to a specific receiver type but works with any given filter.

The transmitter pipeline structure is shown in Fig. 17(a). In each pipeline iteration, M samples of data in the frequency domain are sent through a filter delay chain. Finally, the time domain signal is acquired by IDFT of the frequency samples. Circularity in the frequency domain is achieved by initializing the delay block with the data of the last subcarrier.

Fig. 17(b) illustrates the corresponding receiver structure. Due to a higher bandwidth of the receiver filter, more delays and filter blocks are required. However, these will work in parallel on the FPGA which does not increase the overall delay, but the

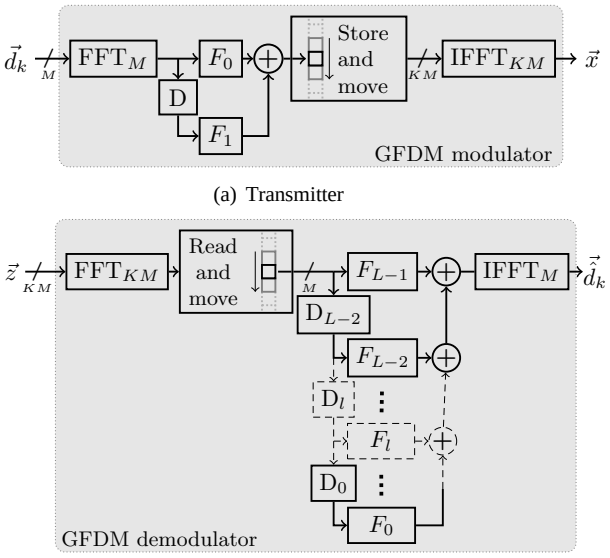

(a) Transmitter

(b) Receiver

Fig. 17: Implementation structure of GFDM transmitter and receiver. D represents a delay of M samples.

TABLE VI: Implementation parameters.

Parameter	Value
Number of subcarriers (K)	$2^{3,4,\ldots,12}$
Number of subsymbols (M)	$2^{3,4,\ldots,7}$
Block length ($N = KM$)	$2^6 \leq N \leq 2^{15}$
Modulation scheme	QPSK, 16QAM, 64QAM
Filter	configurable
Used subcarrier mapping	configurable
Bandwidth	10... 30MHz
CP length	$0 \ldots 3K$ samples

TABLE VII: Compilation results.

Resources	Value
Total Slices	73,3% (10783 out of 14720)
Slice Registers	44,3% (26104 out of 58880)
Slice LUT	48,6% (28642 out of 58880)
DSP48s	19,7% (126 out of 640)
Block RAMs	80,3% (196 out of 244)

occupied area in the chipset. The received time domain signal is first transformed to the frequency domain and then sent through the filter delay chain. The required decimation in time by a factor L is achieved by the summation of the L separately filtered groups before taking the IFFT of the data. Circularity for every subcarrier is achieved by initializing the delay blocks according to $D_l[j] = X[j + (K - L + 1 + l)M]$. At the output of the receiver, the subcarriers are delivered with a delay of $L/2 - 1$ due to the filter bandwidth.

To verify the practical feasibility of the low-complexity GFDM transceiver structure, a software defined radio platform was designated for its implementation. The demonstrator consists of a National Instruments PXI [46] PC-based platform including an Intel i7 general purpose processor (GPP) for controlling the application and performing basic baseband processing and a FlexRIO 7965 FPGA module for high-throughput baseband processing. NI FlexRIO provides user-programmable FPGA modules coupled to interchangeable I/O adapter modules, such as the NI-5791 RF transceiver module. The latter has a continuous frequency coverage from $200\,\mathrm{MHz}$ to $4.4\,\mathrm{GHz}$, $100\,\mathrm{MHz}$ of instantaneous bandwidth on both transmitter and receiver, and performs signal up- and down-conversion to and from radio frequencies. The hardware and software components of this platform are integrated with the LabVIEW graphical programming language.

The GFDM transceiver was fully implemented on the FPGA of the platform, realizing the pipeline structure as described in this section. The parameter configuration in Tab. VI is flexible, which allows to cover a variety of different GFDM applications.

The GFDM implementation makes use of the Xilinx FFT IP core [47]. This IP core supports a pipelined streaming architecture for continuous data processing and a run-time configurable transform point size that can be a positive integer power of two. Compiling the GFDM transmitter for a Xilinx Virtex-5 SX95T FPGA platform uses around 75% of the chip resources. Detailed results of the compilation are presented in the Tab. VII. The digital baseband processing uses a parallel structure with different timed loops and a first-in-first-out (FIFO) memory approach to exchange data among processing blocks. Notice that the design also includes advanced debugging features that allow collection of internal data and the control of system parameters through an external graphical user interface (GUI) developed with LabVIEW. The bottleneck in the system is the loop that feeds the DAC. With typical bandwidths being in the range between $20\,\mathrm{MHz}$ and $50\,\mathrm{MHz}$, the current design is capable to generate GFDM blocks of up to 32768 samples length continuously.

The complete base implementation verifies that GFDM can be implemented with reasonable complexity using today's technology. The prototype is the core of our 5G wireless testbed for experimental research and will be extended by more advanced algorithms and additional PHY layer features, such as framing, channel coding, and data interfaces in the future.

X. Conclusions

A novel modulation proposal for a 5G physical layer needs to address the specific requirements described in this paper. The first key property of a future waveform is flexibility, so that different applications can be addressed by a single solution with different parameter settings instead of multiple solutions. This flexibility includes the partitioning of time and frequency resources, as well as means for spectrum engineering. The latter property is especially useful to control the impact of interference among multiple users and between systems in adjacent frequency bands. It is also important to guarantee a harmonious coexistence with other technologies, as we experience today with 4G networks operating in the so called Digital Dividend. Typically, filtering needs to be introduced on the transmitter or receiver side to achieve coexistence. But doing so, chances are that orthogonality will be forfeit. Nevertheless, the proposed scheme should still be capable of MIMO, and synchronization and channel estimation should preferably be easy to implement. Also error rate performance should not

be neglected, once the focus is shifted towards robustness for certain applications. In this respect, the proposed scheme needs to be as good as state-of-the art orthogonal waveforms, if not outperform them. Lastly, a laboratory proof-of-concept is desirable, in order to validate the feasibility of the proposal. In this work, we have presented GFDM as a candidate waveform modulation scheme for the air interface of future 5G networks. We have shown how the requirements imposed by the different envisioned application scenarios can be addressed with a flexible block structure and subcarrier filtering and have presented suitable parameter configurations for these scenarios. We have introduced two techniques, which in addition to the subcarrier filter address the requirement of low out-of-band radiation and presented a preamble based synchronization scheme that preserves these low spectral emission. We have analyzed the error rate performance of GFDM analytically and numerically for various channel conditions and with iterative receivers, yielding several GFDM configurations that have no penalties compared to OFDM and SC-FDE. We have addressed MIMO-GFDM as a mean to obtain diversity in the system and lastly presented a proof-of-concept implementation.

Certainly, many more issues still need to be resolved. Nevertheless, this paper has shown that GFDM is a novel modulation technology with the potential to fulfill the requirements of the next generation of mobile wireless systems.

REFERENCES

[1] G. Fettweis and S. Alamouti, "5G: Personal Mobile Internet Beyond What Cellular Did to Telephony," *IEEE Communications Magazine*, vol. 52, no. 2, pp. 140–145, Feb. 2014.

[2] G. Wunder, P. Jung, M. Kasparick, T. Wild, F. Schaich, Y. Chen, S. Brink, I. Gaspar, N. Michailow, A. Festag, L. Mendes, N. Cassiau, D. Ktenas, M. Dryjanski, S. Pietrzyk, B. Eged, P. Vago, and F. Wiedmann, "5GNOW: Non-Orthogonal, Asynchronous Waveforms for Future Mobile Applications," *IEEE Communications Magazine*, vol. 52, no. 2, pp. 97–105, Feb. 2014.

[3] Y. Ding, Y. Jin, L. Ren, and K. Hao, "An Intelligent Self-Organization Scheme for the Internet of Things," *IEEE Computational Intelligence Magazine*, vol. 8, no. 3, pp. 41–53, Aug. 2013.

[4] G. P. Fettweis, "The Tactile Internet: Applications and Challenges," *IEEE Vehicular Technology Magazine*, vol. 9, no. 1, pp. 64–70, Mar. 2014.

[5] N. Tadayon and S. Aissa, "Modeling and Analysis of Cognitive Radio Based IEEE 802.22 Wireless Regional Area Networks," *IEEE Transactions on Wireless Communications*, vol. 12, no. 9, pp. 4363–4375, Sep. 2013.

[6] J. Bingham, "Multicarrier Modulation for Data Transmission: An Idea Whose Time Has Come," *IEEE Communications Magazine*, vol. 28, no. 5, pp. 5–14, May 1990.

[7] M. Mirahmadi, A. Al-Dweik, and A. Shami, "BER Reduction of OFDM Based Broadband Communication Systems over Multipath Channels with Impulsive Noise," *IEEE Transactions on Communications*, vol. 61, no. 11, pp. 4602–4615, Nov. 2013.

[8] S. Fechtel and A. Blaickner, "Efficient FFT and Equalizer Implementation for OFDM Receivers," *IEEE Transactions on Consumer Electronics*, vol. 45, no. 4, pp. 1104–1107, Nov. 1999.

[9] J. Kim, J. Lee, J. Kim, and J. Yun, "M2M Service Platforms: Survey, Issues, and Enabling Technologies," *IEEE Communications Surveys & Tutorials*, vol. 16, no. 1, pp. 61–76, 2014.

[10] M. Nekovee, "Quantifying Performance Requirements of Vehicle-to-Vehicle Communication Protocols for Rear-End Collision Avoidance," in *Proc. IEEE 69th Vehicular Technology Conference*, vol. 1. Barcelona, Spain: IEEE, Apr. 2009, pp. 1–5.

[11] H. Kim, J. Kim, S. Yang, M. Hong, and Y. Shin, "An Effective MIMO-OFDM System for IEEE 802.22 WRAN Channels," *IEEE Transactions on Circuits and Systems II: Express Briefs*, vol. 55, no. 8, pp. 821–825, Aug. 2008.

[12] J. Van De Beek and F. Berggren, "Out-of-Band Power Suppression in OFDM," *IEEE Communications Letters*, vol. 12, no. 9, pp. 609–611, Sep. 2008.

[13] E. Hossain, *Dynamic Spectrum Access and Management in Cognitive Radio Networks*. Cambridge University Press, 2009.

[14] B. Farhang-Boroujeny, "OFDM Versus Filter Bank Multicarrier," *Signal Processing Magazine, IEEE*, vol. 28, no. 3, pp. 92–112, May 2011.

[15] V. Vakilian, T. Wild, F. Schaich, S. ten Brink, and J.-F. Frigon, "Universal-Filtered Multi-Carrier Technique for Wireless Systems Beyond LTE," in *9th International Workshop on Broadband Wireless Access (BWA'13) co-located with IEEE Globecom'13*, Atlanta, GA, USA, Dec. 2013.

[16] R. Ayadi, M. Siala, and I. Kammoun, "Transmit/Receive Pulse-Shaping Design in BFDM Systems over Time-Frequency Dispersive AWGN Channel," in *Proceedings IEEE International Conference on Signal Processing and Communications (ICSPC'07)*, Dubai, UAE, Nov. 2007, pp. 772–775.

[17] H. G. Feichtinger and T. Strohmer, Eds., *Advances in Gabor Analysis*, ser. Applied and Numerical Harmonic Analysis. Boston: Birkhauser, 2003.

[18] C. Lélé, P. Siohan, and R. Legouable, "The Alamouti Scheme with CDMA-OFDM/OQAM," *EURASIP Journal on Advances in Signal Processing*, vol. 2010, pp. 1–14, 2010.

[19] G. Fettweis, M. Krondorf, and S. Bittner, "GFDM – Generalized Frequency Division Multiplexing," in *Proceedings 69th IEEE Vehicular Technology Conference (VTC Spring'09)*, Barcelona, Spain, Apr. 2009.

[20] D. Falconer, S. Ariyavisitakul, A. Benyamin-Seeyar, and B. Eidson, "Frequency Domain Equalization for Single-Carrier Broadband Wireless Systems," *Communications Magazine, IEEE*, vol. 40, no. 4, pp. 58–66, 2002.

[21] R. Datta, N. Michailow, M. Lentmaier, and G. Fettweis, "GFDM Interference Cancellation for Flexible Cognitive Radio PHY Design," in *Proceedings 76th IEEE Vehicular Technology Conference (VTC Fall'12)*, Québec City, Canada, Sep. 2012, pp. 1–5.

[22] A. Awoseyila, C. Kasparis, and B. G. Evans, "Improved Preamble-Aided Timing Estimation for OFDM Systems," *IEEE Communications Letters*, vol. 12, no. 11, pp. 825–827, Nov. 2008.

[23] E. Biglieri, *MIMO Wireless Communications*. Cambridge: Cambridge University Press, 2010.

[24] S. Alamouti, "A Simple Transmit Diversity Technique for Wireless Communications," *IEEE Journal on Selected Areas in Communications*, vol. 16, no. 8, pp. 1451–1458, Oct. 1998.

[25] I. Bravo, M. Mazo, J. Lazaro, P. Jimenez, A. Gardel, and M. Marron, "Novel HW Architecture Based on FPGAs Oriented to Solve the Eigen Problem," *Very Large Scale Integration (VLSI) Systems, IEEE Transactions on*, vol. 16, no. 12, pp. 1722–1725, Dec 2008.

[26] N. Michailow, S. Krone, M. Lentmaier, and G. Fettweis, "Bit Error Rate Performance of Generalized Frequency Division Multiplexing," in *Proceedings 76th IEEE Vehicular Technology Conference (VTC Fall'12)*, Québec City, Canada, Sep. 2012, pp. 1–5.

[27] S. M. Kay, "Fundamentals of statistical signal processing: detection theory," 1998.

[28] N. Michailow and G. Fettweis, "Low Peak-to-Average Power Ratio for Next Generation Cellular Systems with Generalized Frequency Division Multiplexing," in *Proceedings International Symposium on Intelligent Signal Processing and Communications Systems (ISPACS'13)*, Naha, Okinawa, Japan, Nov. 2013, pp. 651–655.

[29] B. S. Thomson, J. B. Bruckner, and A. M. Bruckner, *Real Analysis*. ClassicalRealAnalysis. com, 2008.

[30] T. van Waterschoot, V. Le Nir, J. Duplicy, and M. Moonen, "Analytical Expressions for the Power Spectral Density of CP-OFDM and ZP-OFDM Signals," *Signal Processing Letters, IEEE*, vol. 17, no. 4, pp. 371–374, Apr. 2010.

[31] X. Xia, "A Family of Pulse-Shaping Filters with ISI-Free Matched and Unmatched Filter Properties," *IEEE Transactions on Communications*, vol. 45, no. 10, pp. 1157–1158, 1997.

[32] B. Sklar, *Digital Communications: Fundamentals and Applications*, 2nd ed. New York: Prentice Hall, 2001.

[33] M. Matthé, N. Michailow, I. Gaspar, and G. Fettweis, "Influence of Pulse Shaping on Bit Error Rate Performance and Out of Band Radiation of Generalized Frequency Division Multiplexing," in *Submitted to: ICC'14 - Workshop on 5G Technologies (ICC'14 WS - 5G)*, Sydney, Australia, Jun. 2014.

[34] K. Lee and D. Williams, "A Space-Time Coded Transmitter Diversity Technique for Frequency Selective Fading Channels," in *Proceedings IEEE Sensor Array and Multichannel Signal Processing Workshop (SAM'00)*, Cambridge, MA, USA, Aug. 2000, pp. 149–152.

[35] N. Al-Dhahir, "Single-Carrier Frequency-Domain Equalization for Space-Time Block-Coded Transmissions over Frequency-Selective Fading Channels," *IEEE Communications Letters*, vol. 5, no. 7, pp. 304–306, Jul. 2001.

[36] J. van de Beek, M. Sandell, and P. Borjesson, "ML Estimation of Time and Frequency Offset in OFDM Systems," *IEEE Transactions on Signal Processing*, vol. 45, no. 7, pp. 1800–1805, Jul. 1997.

[37] T. Schmidl and D. Cox, "Robust Frequency and Timing Synchronization for OFDM," *IEEE Transactions on Communications*, vol. 45, no. 12, pp. 1613–1621, Dec. 1997.

[38] H. Minn, M. Zeng, and V. Bhargava, "On Timing Offset Estimation for OFDM Systems," *IEEE Communications Letters*, vol. 4, no. 7, pp. 242–244, Jul. 2000.

[39] I. Gaspar, N. Michailow, A. Navarro Caldevilla, E. Ohlmer, S. Krone, and G. Fettweis, "Low Complexity GFDM Receiver Based On Sparse Frequency Domain Processing," in *Proceedings of the 77th IEEE Vehicular Technology Conference (VTC Spring'13)*, Dresden, Germany, Jun. 2013, pp. 1–6.

[40] 3GPP, "Multiplexing and Channel Coding," 3rd Generation Partnership Project (3GPP), TS 36.202, 09 2010.

[41] C. Berrou, A. Glavieux, and P. Thitimajshima, "Near Shannon Limit Error-Correcting Coding and Decoding: Turbo-Codes. 1," in *Proceedings IEEE International Conference on Communications (ICC'93)*, vol. 2, May 1993, pp. 1064–1070 vol.2.

[42] Y.-C. Liang, K.-C. Chen, G. Y. Li, and P. Mahonen, "Cognitive Radio Networking and Communications: An Overview," *IEEE Transactions on Vehicular Technology*, vol. 60, no. 7, pp. 3386–3407, Sep. 2011.

[43] J. Lee, Y. Kim, H. Lee, B. Ng, D. Mazzarese, J. Liu, W. Xiao, and Y. Zhou, "Coordinated Multipoint Transmission and Reception in LTE-advanced Systems," *IEEE Communications Magazine*, vol. 50, no. 11, pp. 44–50, Nov. 2012.

[44] V. Mayer-Schönberger and K. Cukier, *Big data: A revolution that will transform how we live, work, and think*. Houghton Mifflin Harcourt, 2013.

[45] N. Michailow, I. Gaspar, S. Krone, M. Lentmaier, and G. Fettweis, "Generalized Frequency Division Multiplexing: Analysis of an Alternative Multi-Carrier Technique for Next Generation Cellular Systems," in *Proceedings 9th International Symposium on Wireless Communication Systems (ISWCS'12)*, Paris, France, Aug. 2012, pp. 171–175.

[46] N. Instruments. (2014, May 23) Parts of a PXI System. [Online]. Available: http://www.ni.com/white-paper/4811/en/pdf

[47] Xilinx. (2014, May 23) Fast Fourier Transform (FFT). [Online]. Available: http://www.xilinx.com/products/intellectual-property/FFT.htm

Nicola Michailow received his Dipl.-Ing. degree in electrical engineering with focus on wireless communications and information theory from TU Dresden, Germany in 2010. From 2008 to 2009 he worked in the R&D department of Asahi Kasei Corporation, Japan, developing signal processing algorithms for sensor data analysis. Since 2010, he has been research associate at the Vodafone Chair at TU Dresden, pursuing a Dr.-Ing. degree. His scientific interests are focused on flexible and non-orthogonal multi-carrier waveforms for next generation cellular systems. During his time at the Vodafone Chair, he contributed to the FP7 projects 5GNOW, CREW, QOSMOS, EXALTED and was part of the RF Lead User Program with National Instruments.

Maximilian Matthé received his Dipl.-Ing degree in Electrical Engineering from TU Dresden in 2013. During his studies he focused on mobile communication systems and communication theory. He performed his internship at National Instruments Dresden and worked on the design and implementation of a measurement site for LTE test UEs. In his Diploma Thesis he concentrated on waveform design for flexible multicarrier transmission systems. Since 2013 he is with the Vodafone Chair Mobile Communication Systems at Technical University Dresden. Maximilian's research focuses on the design and evaluation of MIMO architectures for future cellular networks.

Ivan Simões Gaspar studied electronic technician (1998) at ETE 'FMC' and received the BSc. (2003) and MSc. (2006) degrees in telecommunications from Inatel. From 2003 to 2011 he was as a technical supervisor and product manager in the R&D department of Hitachi Kokusai Linear S/A, responsible for the design of digital TV transmitters, terrestrial and satellite microwave links and multiplexer equipment operating in single frequency networks. From 2008 to 2011 he was also a lecturer at Inatel. Since February 2012 he is research associate and doctorate candidate at the Vodafone Chair at TU Dresden, working on robust non-orthogonal modulation schemes in the 5GNOW project and in the RF Lead User Program with National Instruments.

Ainoa Navarro Caldevilla received her Dipl-Ing. degree from the University of Cantabria (Spain) in April 2007. She studied telecommunication engineering with keen interest in mobile communications systems and digital signal processing. Through her final thesis in 2007 she was specialized in wireless communications, IEEE 802.11 and network programming. Since March 2009 she is a member of the Vodafone Chair working on projects like EASY-C, FUTON, Artist4G, 5GNOW and RF Lead User Program with National Instruments focusing on system design for embedded systems, software defined radio platforms and FPGA prototyping for signal processing algorithms.

Luciano Leonel Mendes received the BSc. and MSc. in Electrical Engineer from Inatel, Brazil in 2001 and 2003, respectively. In 2007 he received the Doctor in Electrical Engineer degree from Unicamp, Brazil. Since 2001 he is a professor at Inatel, Brazil, where he has acted as technical manager of the hardware development laboratory from 2006 to 2012. He has coordinated the Master Program at Inatel and several research projects funded by FAPEMIG, FINEP and BNDES. He is a post-doc visiting researcher, sponsored by CNPq-Brasil, at Vodafone Chair Mobile Communications Systems at the TU Dresden since 2013. His main area of research is wireless communication and currently he is working on multicarrier modulations for 5G networks and future mobile communication systems.

Andreas Festag received a Dipl.-Ing degree (1996) and Ph.D. (2003) in Electrical Engineering from the Technical University Berlin. As researcher, he worked with the Telecommunication Networks Group (TKN) at Technical University Berlin, Heinrich-Hertz-Institute (HHI) in Berlin and NEC Laboratories in Heidelberg, where he lastly had the position of a Chief Researcher. Since 2013 he is research group leader at the Technical University Dresden, Vodafone Chair Mobile Communication Systems. Andreas has worked on various research projects for wireless and mobile communication networks and published more than 50 papers in journals, conference proceedings and workshops. He actively contributes to the CAR-2-CAR Communication Consortium and to ETSI Technical Committee ITS. He is senior member of IEEE.

Gerhard Fettweis earned his Ph.D. under H. Meyr's supervision from RWTH Aachen in 1990. Thereafter he was at IBM Research and then at TCSI Inc., California. Since 1994 he is Vodafone Chair Professor at TU Dresden, Germany, with main research interest on wireless transmission and chip design. He is an IEEE Fellow and an honorary doctorate of TU Tampere. As repeat entrepreneur he has co-founded 11 startups so far. He has setup funded projects in size of close to EUR 1/2 billion, notably he runs the German science foundation's CRC HAEC and COE cfAED. He is actively involved in organizing IEEE conferences, e.g. TPC Chair of ICC 2009 and TTM 2012, General Chair of VTC Spring 2013 and DATE 2014.